Geophys. J. Int. (2007) **168,** 659–680 doi: 10.1111/j.1365-246X.2006.03178.x

A physically based strong ground-motion prediction methodology; application to PSHA and the 1999 $M_w = 6.0$ Athens earthquake

Lawrence Hutchings,[1] Eleni Ioannidou,[2] William Foxall,[1] Nicholas Voulgaris,[2] Jean Savy,[1] Ioannis Kalogeras,[3] Laura Scognamiglio[4] and George Stavrakakis[3]

[1]*Lawrence Livermore National Laboratory, Hazards Mitigation Center,* PO Box 808, L-201, *Livermore, CA* 94551-0808*, USA. E-mail: hutchings2@llnl.gov*
[2]*Department of Geophysics-Geothermics, University of Athens, Athens* 15783*, Greece*
[3]*Institute of Geodynamics, National Observatory of Athens, Athens, Greece*
[4]*Istituto Nazionale di Geofisica e Vulcanologia, Rome, Italy*

Accepted 2006 August 11. Received 2006 August 10; in original form 2004 November 19

SUMMARY

We present a physically based methodology to predict the range of ground-motion hazard for earthquakes along specific faults or within specific source volumes, and we demonstrate how to incorporate this methodology into probabilistic seismic hazard analyses (PSHA). By 'physically based,' we refer to ground-motion syntheses derived from physics and an understanding of the earthquake process. This approach replaces the aleatory uncertainty that current PSHA studies estimate by regression of empirical parameters with epistemic uncertainty that is expressed by the variability in the physical parameters of the earthquake rupture. Epistemic uncertainty can be reduced by further research. We modelled wave propagation with empirical Green's functions. We applied our methodology to the 1999 September 7 $M_w = 6.0$ Athens earthquake for frequencies between 1 and 20 Hz. We developed constraints on rupture parameters based on prior knowledge of the earthquake rupture process and on sources within the region, and computed a sufficient number of scenario earthquakes to span the full variability of ground motion possible for a magnitude $M_w = 6.0$ earthquake with our approach. We found that: (1) our distribution of synthesized ground motions spans what actually occurred and that the distribution is realistically narrow; (2) one of our source models generates records that match observed time histories well; (3) certain combinations of rupture parameters produced 'extreme,' but not unrealistic ground motions at some stations; (4) the best-fitting rupture models occur in the vicinity of 38.05°N, 23.60°W with a centre of rupture near a 12-km depth and have nearly unilateral rupture toward the areas of high damage, which is consistent with independent investigations. We synthesized ground motion in the areas of high damage where strong motion records were not recorded from this earthquake. We also developed a demonstration PSHA for a single magnitude earthquake and for a single source region near Athens. We assumed an average return period of 1000 yr for this magnitude earthquake and synthesized 500 earthquakes distributed throughout the source zone, thereby having simulated a sample catalogue of ground motion for a period of 500 000 yr. We then used the synthesized ground motions rather than traditional attenuation relations for the PSHA.

Key words: computational PSHA, empirical Green's functions, quasi-dynamic, source models, strong ground-motion prediction, 1999 Athens earthquake.

INTRODUCTION

In this paper, we present a physically based methodology to predict a range of ground motions at a particular site that may occur from a particular magnitude earthquake along a specific fault or within a specific source volume, and demonstrate a means to incorporate this into traditional probabilistic seismic hazard analyses (PSHA). The prediction methodology is based upon the work first presented by Hutchings (1991, 1994) and further developed by Hutchings *et al.* (1996). The physical model proposed by the previous studies has been further developed in this study and the methodology expanded to include PSHA. We apply the methodology to the $M_w = 6.0$, 1999 Athens earthquake. The full methodology is implemented by executing five computer programs: NetMoment,

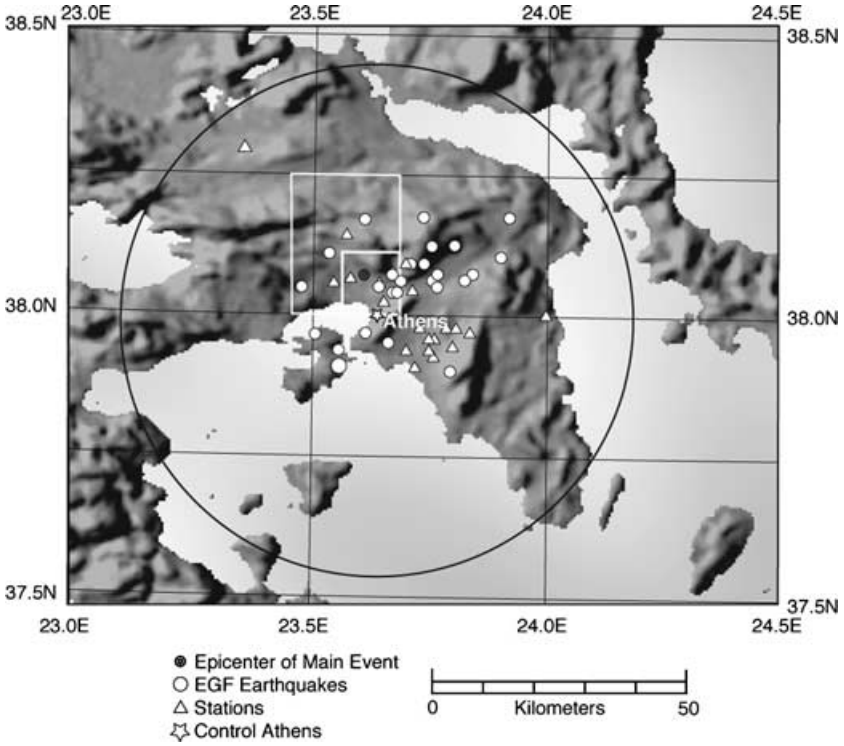

Figure 1. The morphology of the Athens area, the epicentre of the main shock, and the locations of stations used in this study. The circle is the 50-km extent of the demonstration PSHA, and the rectangles are the larger and smaller source zones referred to in the text.

HAZARD, EMPSYN, HazStats and COMPARE. These programs are discussed as appropriate throughout the paper.

By 'physically based,' we refer to ground-motion syntheses derived from physics and an understanding of the earthquake process. We compute ground motions for finite rupture models with the Green's function summation solution of the representation relation that uses synthetic or empirical Green's functions (EGFs). The basic premises of the methodology are as follows. (1) The rupture characteristics of a fault can be constrained in advance by a range of physical parameters. (2) Accurate synthesis of ground motions for a particular fault rupture scenario, sufficient for engineering purposes, is possible from simple rupture models. (3) The range of possible fault rupture scenarios spans the limits of the earthquake process and effectively constrains the range of predictions. (4) The methodology allows one to identify the specific parameters that contribute most to the epistemic variability in the ground-motion predictions; therefore, uncertainty can be reduced with further studies.

We apply the methodology to the 1999 September 7 $M_w = 6.0$ Athens earthquake at six sites. The geology at these sites is competent enough to remain in the linear regime; therefore, we do not address non-linear response at this time. Although the limited amount of data does not allow for a good test of the methodology, we provide a full demonstration and a partial test. First, we chose a relatively small source volume within which the 1999 earthquake is considered to have occurred and computed 57 possible scenarios of the 1999 earthquake. We compared the distribution of synthesized ground motions to observed records of the 1999 event as a partial validation of the prediction methodology. We then determined whether the predicted ranges of absolute acceleration response spectra and Fourier amplitude spectra include the observed records. We found that: (1) our distribution of synthesized ground motions spans what actually occurred and that the distribution is realistically narrow; (2) one of our source models generates records that match observed time histories well; (3) the best-fitting rupture models occur in the vicinity of 38.05°N, 23.60°W with a centre of rupture near a 12-km depth and have nearly unilateral rupture toward the areas of high damage, which is consistent with independent investigations. We also synthesized ground motion in areas that had damage from the 1999 earthquake but did not have strong motion recordings.

We then developed a demonstration PSHA for a single magnitude earthquake and for a single source region near Athens. We identified a larger source volume near Athens within which a magnitude $M_w = 6.0$ is likely to occur, and assumed an average return period of 1000 yr. We synthesized 500 earthquakes to span the complete cyclic history of seismicity and then used the synthesized seismograms rather than attenuation relations to calculate a PSHA. We developed a histogram of peak accelerations to calculate a demonstration hazard curve for Athens. Fig. 1 shows the two source areas and the epicentre of the main event. Fig. 2 shows locations of stations and events used to obtain EGFs in this study.

It is apparent from Fig. 2 that the six stations used to compare synthesized recordings to actual recordings (ATHA, DMKA, FIXA, THVC, SGMA and SPLA) of the 1999 main event have limited azimuthal distribution, so full analysis of rupture models is not reliable. The observed records were near the upper limit of our range of syntheses, and it is not clear whether this is because the azimuthal range of recordings was in an area of unusually high values or due to other possible explanations discussed below. We also found that certain combinations of rupture parameters produced 'extreme', but not unrealistic, ground motions at some stations and these values are capped for longer return periods. This is in contrast to traditional PSHA calculations where 'extreme' values continue to increase with increasing return periods.

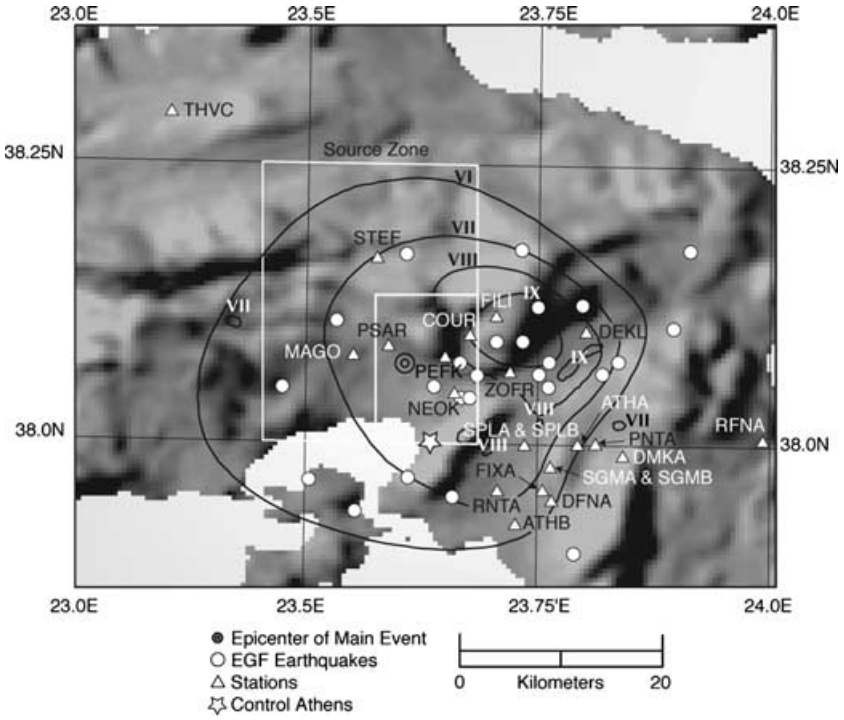

Figure 2. Isoseismal intensity from the earthquake in modified Mercalli scale. The rectangles are the larger and smaller source zones referred to in the text.

Physically based probabilistic hazard approach

Historically, strong ground-motion prediction has generally taken one of two paths: probabilistic or deterministic. Here, we have combined the two methods into a new approach for probabilistic seismic hazard studies. Following Cornell (1968), state-of-the-practice, probabilistic seismic hazard analyses require: (1) an interpretation of seismic sources that constitute a hazard to a particular site so that the distances of earthquakes from the site can be determined; (2) an interpretation of earthquake recurrence for each source; (3) models of ground-motion prediction in the form of regional attenuation relationships. (4) Given these input evaluations, the PSHA method integrates over all values of the variables and produces an estimate of the mean yearly frequency of exceedance for ground-motion amplitude at the site (i.e. a hazard curve). Alternatively, a deterministic approach identifies significant faults or source zones and estimates the ground motion for some maximum value of the magnitude of earthquakes occurring at the source. Deterministic hazard studies have had the problem of not identifying the inherent variability in the location and size of earthquakes, leaving possible irresolvable disagreements between experts. Probabilistic studies characterize uncertainties well, but rely on very simplified characterization of the hazard.

In this paper, we use deterministic studies by calculating actual earthquake rupture and ground motion relevant to a particular site, and incorporate the results into PSHA studies by replacing attenuation relations. We generate rupture scenarios that span the variability of potential ground motion in a predictive situation. In a full application, all sources and all magnitudes would be included, and all physically based earthquake models would be employed to capture the full epistemic uncertainty of the problem. The output from this PSHA approach is a library of source- and site-specific ground-motion time-series comprising a sample of all the earthquakes that could affect a site during its design life. The library of seismograms can be used either to develop hazard curves of traditional engineering parameters in the form of the annual probability of exceedance or to develop risk estimates that can be directly applied in building design. Our methodology assumes linear response, so that it represents rock or firm soil sites. Heuze *et al.* (1994) demonstrate a means to incorporate this methodology with non-linear soil models.

The methodology proposed is essentially that recommended by the Southern California Earthquake Center, Phase III study (Field *et al.* 2000). This study concluded that the complex propagation effects unique to earthquake-rupture/site combinations result in uncertainties. Therefore, the standard empirical-regression method must be replaced with one that uses a more physics-based approach to ground-motion modelling. This approach has further been endorsed by the National Research Council (2003). A good framework with which to implement the approach on a large scale has been proposed by Field *et al.* (2003). Convertito *et al.* (2006) proposed a similar approach as discussed in this paper.

Problems with current PSHA approaches

In traditional PSHA, ground motion at a particular site is determined from attenuation relationships. These relationships are usually derived empirically from the strong-motion database of past earthquakes. These relationships are simple functions of earthquake magnitude and source–site distance with, in some cases, a few additional source parameters. Our basic premise is that for near source regions fifty years of strong-motion records worldwide is insufficient to capture the range of site and propagation path conditions, rupture processes and geometric relationships between source and site that are possible from earthquakes. For example, prior to the 1999 Chi Chi, Taiwan, and 1999 Turkey earthquakes, only 20 high-frequency ground-motion recordings were available worldwide for

earthquakes with magnitude >7 and at a distance <20 km from the fault (Abrahamson & Shedlock 1997). The Turkey earthquake added seven and the Taiwan earthquake added 65 (Lee *et al.* 2001) recordings. Nonetheless, only two fault rupture scenarios were added.

The uncertainty in ground-motion estimates is expressed as standard probability distribution in the attenuation relationships, which are not correlated with the properties for the region of interest. Rather, they are arbitrary distribution functions, usually lognormal with asymptotic tails for high values. The uncertainty in a ground-motion relationships arises from the variability in source characteristics among events of the same size in the strong-motion database and from the different earth structures through which the seismic waves from the events propagated. In PSHA studies, this is considered aleatory uncertainty, the uncertainty due to inherent randomness of the process. Current PSHA studies are based upon the ergodic assumption that the randomness in space from several sources throughout the world (or region) is the same as the randomness in time from the same source (Anderson & Brune 1999). With the ergodic assumption, correlation between the ground motion and the specific source, path and site is lost, thereby leading to potentially higher total uncertainty in hazard estimates than if each earthquake source release of energy were individually propagated to the site of interest. There is also an attempt to model epistemic uncertainty, the uncertainty in knowledge about the earthquake processes. This refers to factors such as strike, dip and slip vector. However, the uncertainty in published relationships has not decreased since 1972 (Fig. 10 in Douglas 2003).

Current PSHA methods were developed in large part to meet licensing needs for nuclear power plants. In this application, annual probabilities of exceedance of ground-motion parameters of interest (e.g. peak and spectral accelerations or spectral velocities) are in the range of 10^{-3} to 10^{-4}. Because the recurrence intervals of the dominant contributing earthquakes are generally in the range of a few hundred to a few thousand years, the ground-motion estimates are generally sampled from the central region of the probability distributions on the ground-motion attenuation relationships or at most from the beginnings of the tails of the distributions. However, licensing practices for sensitive structures that require estimation of ground motions with annual probabilities of exceedance of 10^{-5} to 10^{-8} inevitably lead to sampling the virtually unconstrained tails of the ground-motion probability distributions. The resulting estimates of ground motion can be extremely high and are physically unrealizable. However, there is at present no generally accepted method either to better characterize the tails of the distributions or to truncate them at some upper boundary of ground motion (Bommer *et al.* 2004).

Additionally, ground-motion syntheses approaches that are not physically based and have been adjusted to fit the historic database, or approaches that fit target spectra obtained from regression with the historic database have the same problem as empirical attenuation relations. Such models have little or no physical basis and can only 'predict' what has been recorded in the past. We propose that with a physically based approach, a better use of the current strong-motion database would be to validate models of the earthquake rupture process and wave propagation.

Advantage of physically based PSHA

A physically based PSHA method offers four advantages. First, the methodology is source- and site-specific; therefore, ground motions at a particular site include the geometric relationships to sources, and results will include the finite faulting effects. If EGFs are also used, then actual propagation path and site effects will be included in the results. Second, the physically based approach relies on physical parameters to model sources; additional research on these parameters will provide better characterization of the variability and possibly reduce it. This approach replaces the aleatory uncertainty that current PSHA studies estimate by regression of empirical parameters with epistemic uncertainty that is expressed by the variability in the physical parameters of the earthquake rupture process. This will naturally define the shape at the tails of the distribution curves and truncate the distributions of ground motions, thereby limiting 'extreme' ground motions. Certainly, a major area of research in the future will be identifying the significant parameters and determining their range. Source rupture parameters are not well known in most regions, and the distribution of parameters must reflect the uncertainty of these parameters based upon physical arguments. Third, because rupture models are physically based, ground motions that have not yet occurred or been recorded will be included in the syntheses. Finally, because input parameters are correlated through a physical model, unrealistic combinations that cannot happen in nature are excluded.

Two examples illustrate the advantage offered by physically based models. The first is the modelling of ground motion that may have occurred in the uninstrumented area of the interchange between California State Highway 15 and Interstate I-5, which failed as a result of the 1994 Northridge, California, earthquake (Hutchings & Jarpe 1996). When those ground motions were used to analyse the failure of the structure and possible replacement designs (Fenves & Ellery 1998), they included a large fault normal pulse that resulted in an extra 'bump' at about 1 s in the pseudo-acceleration response spectra. This bump was not considered by other empirically based methodologies and was not observed by nearby acceleration sites that were not on the strike of the fault (figs 2.18 and 2.19 in Fenves & Ellery 1998). The second example is the fault rupture models used to 'predict' the ground motion that may occur at the San Francisco/Oakland (California) Bay Bridge from an $M_w = 7.25$ earthquake (Hutchings *et al.* 2005). These models generated long-period tectonic 'fling' pulse shapes that had not been previously observed until the 1999 Turkey earthquake; however, such a response would significantly affect the bridge response (McCallen *et al.* 2006).

Rupture models

In our proposed methodology, rupture models are consistent with the elastodynamic equations of seismology and fracture energy and with a physical understanding of how earthquakes rupture. They also are consistent with results from laboratory experiments, numerical modelling and field observations of earthquake processes. These models are often referred to as quasi-dynamic models (Boatwright 1981). Our source model is one of a family of such models; others include Boatwright (1981), Hartzell (1982), Heaton (1982), Papageorgiou & Aki (1983), Spudich & Frazier (1984), Cohee *et al.* (1991), Zollo *et al.* (1997) and Guatteri *et al.* (2003).

The ultimate solution for modelling earthquakes would be dynamic solutions that satisfy elastodynamic equations and fracture energy and have known elastic constants and constituent relations for the faulting process. However, these parameters are very uncertain in the fault zone, and several poorly bounded assumptions must be used. The resulting uncertainties in computations make their usefulness limited to better understanding the earthquake process and providing bounds for quasi-dynamic rupture models.

METHODOLOGY

Rupture model

Our rupture model is implemented by the computer code EMPSYN, which calculates synthetic seismograms by numerically computing the discretized representation relation with empirical Green's functions (EGF). It uses the form (Hutchings & Wu 1990; Hutchings 1991) for synthesized ground motion:

$$u_n(X,t) = \sum_{i=1}^{N} \frac{\mu_i A_i S(t')_i}{M^e_{0i}} * e_n(X, t' - t_r)_i \tag{1}$$

where (X, t) are position and time in space relative to the hypocenter and the origin time of the synthesized earthquake. N is the number of elements and i refers to values at an element. A_i is an elemental area such that $\sum A_i$ equals the total rupture area. μ_i is the rigidity at an element. $S(t')_i$ is the desired slip function at an element analytically deconvolved with the step function. $e_n(X, t')_i$ is the recording of a small earthquake with effectively a step source time function, and interpolated to have a source and origin time at the location of the ith element. t' is relative to the origin time of the synthesized eqrthquake. t_r is the rupture time from the hypocenter to the element, which is the integral of radial distance from the hypocenter of the synthesized earthquake divided by the rupture velocity, which can be a function of position on the fault. M^e_{0i} is the scalar seismic moment of the source event, and $*$ is the convolution operator. u_n has the same units as e_n.

The EGF approach offers three main advantages. If the EGFs are available and managed properly, they provide the exact elastodynamic Green's function for the real earth and the exact rigidity at the source. In addition, they do not require empirical scaling relations between large and small earthquakes. Following Aki & Richards (1980, section 3.2), solving the representation relation for an impulsive point source, with a scalar source time function, gives the equation for an empirical Green's function as:

$$e_n(X,t) = \mu^e A^e \bar{s}^e (\hat{s}_p \hat{n}_q + \hat{s}_q \hat{n}_p) H(t') * G_{np,q}(X, t; \chi, t') \tag{2}$$

where $\mu^e A^e \bar{s}^e$ is the rigidity, area, and average slip at the source of the EGF and is equal to M^e_{0i} in eq. (1); $(\hat{s}_p \hat{n}_q + \hat{s}_q \hat{n}_p)$ is the focal mechanism and $H(t')$ is the step source time function of the EGF at location χ and origin time at $t' = 0$; and $G_{np,q}$ is the elastodynamic Green's function. Plugging eq. (2) into eq. (1), one can see the familiar representation relation, where the step function is removed by the deconvolution that is included in the source time function of the main event. At this point, the focal mechanism solutions of the large and small events are assumed to be the same, and the source locations of the EGFs are at the element locations. Also, from eq. (1), the amplitude of the EGF is scaled linearly for the desired contribution from the elemental area by the ratio of the moment of the elemental contribution to that of the EGF. This scaling does not affect the solution's integrity as long as the EGF has a source corner frequency higher than the frequency of interest. This is an exact solution for the representation relation for these conditions. Our intent is to remain as close as possible to the mathematically exact solution, because approximations add to the uncertainty of the solution. This modelling approach only requires that the number of times small earthquakes are used in the synthesis be such that the sum of their moments adds up to the moment of the large earthquake. Therefore, low-frequency amplitudes match those of observed seismograms. The high frequency is matched simply by using appropriate rupture parameters (Hutchings 1994).

We use the Kostrov slip function in EMPSYN. It was derived from the analytical solution for rupture of a circular crack in a homogeneous medium (Buridge & Willis 1969):

$$K(\chi, t) = \frac{0.81\sigma\beta}{\mu}\left(t^2 - t_r^2\right)^{1/2} \tag{3}$$

where β is the shear wave velocity, 0.81 is a constant used for V_r equal to 0.9 β, μ is rigidity and σ is stress drop. This expression does not include healing or termination of the slip. We transform the Kostrov function to be relative to element time t'. Making this transformation to eq. (3), adding healing, and deconvolving out a step function, the Kostrov slip function at an element in eq. (1) becomes:

$$S(t')_i = \frac{1}{H(t')} \oplus \frac{0.81\sigma_i\beta_i}{\mu_i}(t'^2 + 2t_r t')_i^{1/2} \tag{4}$$

for time at the element from 0.0 to τ_o (the rise time). The rise time in EMPSYN is determined by the shortest time for the rupture front to reach the fault edge and a healing phase to then reach the element. Now, t_r puts a rupture distance dependence on eq. (4), and for long faults, it causes $S(t')_i$ to increase with spatial separation from the hypocenter. To constrain this, we limit t_r to be equal to or less than the rupture time to the nearest edge. This constraint is subjective and a departure from a pure crack solution for an extended rupture. When eq. (4) is plugged into eq. (1), the synthetic rigidity cancels out, leaving the actual rigidity at the source location of the EGF.

We diminish rigidity and stress drop proportionally near the surface in relation to the lithostatic load. This has two effects. First, reducing the rigidity results in very little moment contribution for rupture near the surface. Second, the commensurate diminishing of stress drop and rigidity results in significant displacements (although not significantly seismogenic) at the surface.

EMPSYN uses a summation of step functions to model the Kostrov slip function in the time domain. The time delay for the step functions' summation is at the digital sampling rate of the EGFs to ensure that high-frequency artefacts are higher than the frequency range of interest. In the frequency domain, EMPSYN employs a ramp function with all the parameters of the Kostrov slip function. Hutchings (1994) showed that the difference in computed seismograms using the ramp to model the shape of the Kostrov slip function was indistinguishable in the frequency range of 0.5 to at least 15.0 Hz.

Green's functions

We use the definition of EGFs, as outlined by Hutchings & Wu (1990), to be recordings of effectively impulsive point sources. 'Effectively impulsive point source' refers to the observation that factors such as rise time, rupture duration, or source dimension are small enough that their effect cannot be observed in the frequency band of interest. Also, stress drop changes are reflected only in the differences of their seismic moment. As such, their displacement source spectra are flat up to the highest frequency of interest, and scale linearly for differences in seismic moments. We perform the following adjustments when appropriate EGFs are not available. If events are not sufficiently small enough to provide impulsive point sources, we deconvolve out their finite Brune source to effectively create impulsive point source events (as demonstrated below). We interpolate all available EGFs to provide the Green's function for each element. We interpolate focal mechanism solutions if they vary from the main event. These steps introduce error, as discussed below and in Hutchings & Wu (1990).

Although we did not model low frequencies in this study, we recommend employing numerical Green's functions at low frequencies (<1 Hz). They can be accurately calculated at these frequencies because only coarse spatial resolution is needed in the geologic models. At high frequencies (>1 Hz), where the spatial scale of variability in the geology does not permit accurate deterministic modelling, we use EGFs to capture the short-wavelength complexity in the path. We recommend the methodology of Jarpe & Kasameyer (1996) for merging high- and low-frequency Green's functions for full broadband solutions.

In many cases, empirical Green's functions are not available. For these situations, we propose: (1) interpolating EGFs to different site locations, if used with caution; (2) constraining numerical Green's functions with site response functions (Hutchings & Wu 1990); or, (3) using stochastic time-series (Boore 1983) with an impulsive point source spectra shaped by attenuation, geometric spreading and site-dependent κ, which can be obtained by analyzing local seismicity (Scognamiglio *et al.* 2005). Of course, if no seismicity data are available, fully synthetic Green's functions may be used.

Variability in rupture models

Variability in rupture models is provided by the compute program HAZARD. HAZARD randomly selects values for rupture geometry, hypocenter location, number and size of asperities, rupture and healing velocity and rupture roughness from even distributions; and strike, dip and slip vector from triangular distributions about preferred values. Moment is fixed for a particular set of rupture scenarios. Rise times, stress drop and energy are dependent variables. We use data from summary studies to constrain some parameters (identified below). Although it is our desire not to depend upon regression of past earthquakes for modelling, some parameters may well be characterized using the ergotic assumption.

Our syntheses show that the ground-motion variability obtained with different models is about the same for different frequencies. This correspondence is apparent in Figs 7 and 8. In our models, the high-frequency variability is due to short wavelength (asperities) or short time duration (rise times and roughness variability) along the fault rupture zone. However, longer scale changes due to focal mechanism radiation variation or long-scale-length finite fault effects, such as directivity and moment distribution, also cause a variability in the low frequencies. The historical database for peak accelerations, for example, shows approximately the same variability for low (<5 Hz) and high frequencies (>5 Hz). Campbell & Bozorgnia (2003) examined strong-motion data recorded for 960 accelerograms from 49 events recorded between 1957 and 1995. They found that the degree of variability in acceleration response spectral ordinates is about the same for periods of 0.1, 1.0 and 3.0 s at distances less than 30 km from the fault (their fig. 5), similar to distances in this study. However, they show a distribution of a factor of approximately ± 7, whereas we show a factor of approximately ± 5. However, our results are for a single fault and a single station, and theirs are from many faults and many stations.

Variability in parameters

Geometry is rectangular for faults that rupture through the entire crust; otherwise, it is elliptical. The shape is determined by examining the slip distributions of previous earthquakes (Hartzel, many references; Wald, many references). Elliptical geometries vary in eccentricity between 0.0 and 0.95.

Slip distribution is varied in two ways. First, the Kostrov slip model with healing (Hutchings 1994) has variable rise times and slip amplitudes on the fault but constant stress drops. As a result, portions of the fault have high slip amplitudes. Second, smaller areas with high slip amplitudes and high stress drops are modelled. These areas, called asperities, are not allowed to overlap. Fault displacement for asperities grade from the value of background rupture at the edge to greatest at the centre. We use Somerville *et al.* (1999) to constrain the average area of slip with amplitude greater than 1.5 times the overall average slip amplitude to be about 20 per cent for the average of all models. The range for our models is between about 10 and 40 per cent of the total fault area. Somerville *et al.* (1999) examined slip distributions from inversion results, primarily from Hartzell and/or Wald (many references), to characterize slip distributions and found that slip amplitudes greater than 1.5 include 20.67 per cent of the total fault surface from regression with all their data.

Asperities are circular in shape and have slip distributions defined by the Kostrov rupture with healing. The number of asperities is randomly chosen to be between 0 and 7. Although the number of asperities is roughly independent of the size of the earthquake, their relative size scales with the fault dimensions. This process replicates observation with inversion studies, which indicate that relatively smaller asperities are not significant to the ground motion of larger earthquakes.

Rise time varies at each point on the fault and is a dependent variable.

Rupture initiates at the arrival time of the rupture front. It continues for the shortest amount of time it takes the rupture front to reach a fault edge and a healing phase to travel back to that point at the healing velocity. Healing phases are not permitted from the surface, where there is little seismogenic rupture. Our healing model is derived from dynamic rupture models (Kostrov & Das 1988, and many others).

Rupture roughness is the percentage of elements at the rupture surface for which we applied randomness to the rise time so that we could simulate roughness. The percentage is randomly selected to be 0, 10, 20, 33 or 50 per cent. For this percentage of elements, rise time is randomly shortened to be between 0.1 and 0.9 times the original value. Roughness is implemented by delaying an element's rupture time so that it finishes slip (rise time) at the same time as neighbouring elements. Areas of roughness have corresponding high stress drop (i.e. the Schultz 2002, model of contact asperities). Asperities and background elements have the same percentage of elements with roughness.

Rupture velocity is allowed to vary between 0.75 to 1.0 times the shear wave velocity, as derived from dynamic rupture modelling (Das & Kostrov 1990, and many others).

Healing velocity is a percentage of the rupture velocity. If the healing velocity is greater than the rupture velocity, it will shortly overtake the rupture front, and no rise time will develop. We randomly varied healing velocity to be between 0.8 and 1.0 times the rupture velocity, which is approximately between the Rayleigh-wave velocity and the shear wave velocity, as observed in dynamic rupture modelling.

Stress drop is a dependent variable derived from the Kostrov slip function. In this derivation, stress drop is that which results in a strain discontinuity and a displacement on the fault, and results in seismic radiation. It is equivalent to the Orowan stress drop (Orowan 1960). Our kinematic models use four effects to vary stress drop in rupture. First, the overall average stress drop is directly dependent upon the moment and size of the rupture area. Second, rupture roughness (described above) results in small areas of relatively high stress

drop. Third, asperities are allowed to have a different stress drop than surrounding portions of the fault rupture; and fourth, stress drop is constrained to diminish near the earth's surface at the rate of $10 + 0.75$ times the confining pressure due to the lithostatic load (300 bars at 1.7-km depth). The minimum of either this value or the full rupture stress drop is used. Typically, stress drop for the main event ranges from 1 to 100 bars, while asperities range from 50 to 500 bars.

Hypocenter depth is limited to be within the lower half of the rupture area because large earthquakes are theoretically predicted to nucleate at depth (Sibson 1982; Tse & Rice 1986). Also, hypocenters are limited to be greatar then the distance from a fault edge to limit strain to be less than 10^{-2}. This distance is generally greater than 100 m for $M > 6$ earthquakes.

Energy is calculated for each fault rupture model by the integral of slip amplitude and stress drop (Schultz 2002) to identify possible unrealistic models, as suggested by Tumarkin (1997). We used calculations of the effective stress as the ratio of moment to energy to identify rupture models that have unrealistic energy. Models are allowed to have effective stress values between 0.05 and 50 MPa. This range is considered broad enough that it does not eliminate any possible extreme events, only the unrealistic events. Generally, we do not find unrealistic events with our rupture models.

Parameter sensitivity

Wossner *et al.* (2002) used EMPSYN to determine how changes in the source parameters affect acceleration time-series and Fourier amplitude spectra. They synthesized seismograms for a strike-slip earthquake of the size and at distances similar to the earthquake studied in this paper. They found that hypocenter location greatly affects the amplitudes of synthesized records from near-source stations because of a directivity effect. On average, amplitude increases by a factor of about 3 for rupture toward either hard rock or soft soil sites (up to a factor of 8 for particular frequencies). In addition, the relation between fault geometry and hypocenter positions significantly affects rise-time distributions and, thus, amplitude and frequency content of the signal. When the hypocenter is located closer to a fault edge, amplitude increases up to a factor of 3 because rise times are shortened. Wossner *et al.* also observed variations in rupture velocity by keeping the ratio of rupture to healing velocity constant (to remove the effect of rise time) and observed up to a factor of 5 variations in amplitudes (and up to 10 at specific frequencies) of synthesized time-series.

Scognamiglio & Hutchings (2006, submitted to the BSSA) modelled ground motion for a hypothesized $M_{\rm w} = 6.0$ earthquake with normal faulting at distances similar to those in this report. They then examined synthesized ground-motion sensitivity to the number and dimension of the asperities, the percentage of roughness on the fault plane, strike, dip and hypocenter position. They found that the number of asperities plays a dominant role in affecting the amplitude of the acceleration time-series. Moving from no asperities to the maximum allowed by the fault dimension (four in their study), the waveform's amplitude decreased up to a factor of 4 at some stations. This decrease is apparently due to a redistribution of energy in the synthesized seismograms so that focusing is diminished.

Similar to Wossner *et al.*, Scognamiglio & Hutchings verified that changing the hypocenter location affects mostly the amplitudes of near-source stations. So, at the closest station (5 km), changing the hypocenter location caused waveform amplitudes to change by a factor of 2, and in the farthest station (21 km), the waveform's amplitude changed by a factor of 1.2. They also found that the computed spectra varied up to $\pm$ a factor of about 2 from the mean when the dip and strike span characteristic values of the studied region.

Additionally, according to Wossner *et al.* (2002), the number of EGFs affects the amplitude of synthesized seismograms. They found that when frequencies are higher than the source corner frequency, these amplitudes tend to be higher if a single EGF is used to interpolate records over the fault. They achieved more stable and reliable results by using at least five EGFs.

Sensitivity to moment of EGFs. Pavic *et al.* (2000) identified the estimation of the EGF moment as the most sensitive parameter for a synthesis approach that is essentially the same as EMPSYN. Amplitude of synthesized seismograms scale inversely with the moment estimation of EGFs (eq. (1)). Accurate calculation of moment is difficult. In the Aki and Richards equation for moment used in this study (their Section 4.5.3), moment is dependent upon seismic velocity raised to the 4th power (we calculate density from the P-wave velocity). A difference of 20 per cent in velocity, for example, changes moment by a factor of approximately 2.4. Wossner *et al.* (2002) used the program EMPSYN to repeatedly calculate synthetic seismograms from 24 source models using either one or several EGFs and found a systematic bias in synthesized seismograms if only one EGF was used. They also found that this bias most likely results from an inaccurate moment calculation. They concluded that using several EGFs averaged out the uncertainties. Dan *et al.* (1990) estimated the uncertainty in synthesized seismograms due to using only one EGF by modelling with 17 different aftershocks. Using the program NetMoment (used in this study, below), Gok & Hutchings (2006) estimated moment and source corner frequency for about 200 aftershocks of the 1999 Anatolian earthquakes recorded at 44 stations. When they compared results of 20 events with those obtained from full *S*-waveform moment tensor inversion and from coda estimates, they found that estimates from NetMoment are within 5 per cent agreement. Gok & Hutchings (2006) calculated the standard deviation of a lognormal distribution of the moment calculation for individual stations compared to the simultaneous inversion results to be a factor of 2.7.

Sensitivity to source corner frequencies of EGFs. Corner frequencies used to deconvolve the finite Brune source from the EGFs (below) can result in inappropriate high or low frequencies in the synthesized seismograms. Source corner frequencies of small events are difficult to determine because site response frequently occurs over the same frequency band as source corner frequencies, and there is often a trade-off with κ (Gok & Hutchings 2006). Gok *et al.* used an f test to determine the range of source corner frequencies that are within 95 per cent confidence limits when a trade-off with κ is tested and found NetMoment-calculated corner frequencies have uncertainties of about $\pm$25 per cent. Finally, they compared corner frequencies of 10 events to those obtained with the parameter-less approach based upon coda analysis of Mayeda *et al.* (2003) and found an overlap of calculations with NetMoment.

Prediction range

The prediction range of ground motion is provided by the computer program HazStats. We assume the following: the scenario earthquakes are all of equal probability; the hazard to a site is monotonic with the hazard parameters; and the scenarios are randomly selected within the bounds of possible rupture parameters. In the terminology of Abrahamson *et al.* (1990), our prediction uncertainty has three

elements: (1) parametric uncertainty, which arises from uncertainty as to which scenario will occur; (2) modelling errors that occur when the actual rupture process is not modelled correctly; and (3) random errors caused by factors such as uncertainties in source parameter estimates for EGFs, interpolation of source events along the fault surface, and uncertainties in estimates of the lognormal mean and standard deviation of the distribution of the scenario earthquakes.

The hazard is defined by the absolute acceleration response (AAR), Fourier amplitude spectra (FAS), peak acceleration (PA), peak velocity (PV), or any chosen parameter of the synthesized ground motions. The estimation of the median (lognormal mean) hazard is:

$$\hat{H}_j = \frac{1}{N}\sum_{i=1}^{N} \log(R_{ij}), \tag{5}$$

where R_{ij} is the hazard parameter (i.e. AAR, FAS, PA, or PV). The index i ranges over the number of scenarios N, while j increments over periods for which AAR and FAS have been evaluated, or are equal to one for PA and PV, etc. The estimation of the 84th percentile (i.e. the average plus one standard deviation) is the combined effect of the prediction errors, and assuming the errors in the mean and standard deviation are independent (Hald 1952):

$$H_j^{\sigma} = \hat{H}_j + \left[\sigma_p^2 + \sigma_m^2 + \sigma_e^2\ N^e + \sigma_r^2\right]^{1/2}, \tag{6}$$

where σ_p^2 is the parametric uncertainty, obtained from the variance of the distribution of hazard parameters and is calculated by HazStats from the ground motions synthesized by EMPSYN for the scenarios chosen by HAZARD. This is generally about 0.3. σ_m^2 accounts for modelling errors when the exact scenario is known but not modelled correctly and for random errors due to interpolation of EGFs. HazStats currently assumes this error to be equal to the standard deviation obtained by Jarpe & Kasameyer (1996) by comparing computed and observed records for the 1989 Loma Prieta earthquake whose independent parameters were well documented. Their average variance over several frequencies is 0.0795. σ_e^2 is the random error uncertainty; we identified this to be primarily due to inaccurate moment calculations. We estimate this error to be 0.0196 for one EGF from examination of the literature (above). This is diminished by one over the number of EGFs, $N^e\sigma_r^2$ is uncertainty in the computation of both the lognormal mean and the standard deviation. HazStats uses a value of 0.0011 obtained by Hutchings *et al.* (1996). Generally, the sum of these variances is about 0.4, a factor of about 4 above the mean.

Previous validations

EMPSYN has been validated by synthesizing an idealized earthquake with the same parameters used by a similar synthesis approach conducted at the University of California at Santa Barbara (UCSB) (Liu, personal communication, 1999). Liu's results were essentially identical to the EMPSYN calculation. Hutchings (1994) also synthesized an expanding circular crack solution and matched the analytical solution. Jarpe & Kasameyer (1996) used Loma Prieta earthquake data to systematically validate the ability of EMPSYN to compute realistic source models. In those validations, they fixed the moment, focal mechanism solution, slip distribution and geometry from independent studies and modelled the observed strong ground motion at 26 sites. They found that the standard error between observed and predicted response spectra is less than or equal to other methods for periods between 0.05 and 2.0 s and is significantly less than regression methods based on pre-Loma Prieta empirical strong-motion data at periods between 0.5 and 5.0 s.

To include the variability resulting from not knowing the source, Hutchings (1991) modelled several rupture scenarios along a segment of the fault for a particular moment. With this calculation, he 'predicted' strong-motion parameters of peak acceleration and pseudo-velocity response at five sites that recorded the Loma Prieta earthquake. He then used 25 rupture scenarios along the fault where the Loma Prieta earthquake occurred to account for the source variability from not knowing the source prior to the earthquake's occurrence. The engineering parameters were predicted within the 16 and 84 per cent lognormal standard errors at four of the five sites. The fifth site had recorded motion just above the one standard error value for both peak acceleration and pseudo-velocity response. Other tests and validations include Hutchings (1994), Foxall *et al.* (1994), Hutchings *et al.* (1997, 1998) and Scognamiglio (2004). Hartzell *et al.* (1999) examined several approaches but did not include the empirical Green's function convolution approach used in this study.

APPLICATION TO THE 1999 ATHENS EARTHQUAKE

Data analysis, observations, and site conditions

The 1999 September 7 $M_w = 6.0$ Athens earthquake occurred about 20 km from the centre of Athens at the western boundary of the greater metropolitan area. It was the first moderate-to-strong earthquake ever to have been reported at distances less than 30 km from the centre of the metropolitan area (Makropoulos *et al.* 1989; Papazachos & Papazachou 1997). About 100 buildings collapsed, which caused 143 casualties (Papadopoulos *et al.* 2000). Most damage was in areas surrounding the metropolitan centre of Athens. The absence of strong seismic events throughout the city's history led scientists to conclude that the greater area of Athens had low seismicity. Several strong-motion recordings were obtained in central Athens, but no strong-motion records were obtained from the high-damage area northwest of Athens (Papadopoulos *et al.* 2000). A critical question is: what ground motion may have occurred in high-damage areas of the 1999 earthquake? Also, what capabilities exist to predict the ground motion of future earthquakes, possibly closer to the centre of Athens?

Intensity and damage to engineering structures

Fig. 2 shows the isoseismal intensity from the 1999 Athens earthquake as it has been compiled by Protonotarios (1999) and Ioannidou *et al.* (2001). The names and locations of stations used in this study are also shown in Fig. 2 and are listed in Table 1. Most of the damage occurred within a 10-km-diameter area, centred about 10 km northeast of the epicentre. Projection up-dip of the proposed fault plane (and hypocenter) would intersect near the high-damage area. Severe damage decreased rapidly with distance from the centre of damage. In most areas of Athens, damage was non-structural and consisted mainly of cracks to in-fill brick walls. All classical monuments survived the earthquake without significant damage (EERI 1999). Some columns at the Acropolis rotated slightly and small pieces of marble fell, but archaeologists considered these damages to be of minor importance. Cracks and minor landslides occurred on the road leading to the summit of Parnitha Mountain, near the epicentre. No other damage was reported on highways, roads, or railroad tracks. Underground pipelines were apparently undamaged. The recently constructed natural gas network was not damaged,

Table 1. Station information.

Station	Latitude (°N)	Longitude (°E)	Location	Orient. l, .t + 90.0	No. EGF	Geol. class
ATHA^{+}	38.00	23.77	Neo Psihiko; 3-story reinforced concrete (RC); −13 m	N180°E	16	c
ATHB^{++}	37.93	23.70	Neo Faliro; planetarium, 3-story RC	120°	4	c
COUR**	38.10	23.65	Fili; soccer stadium	0°	5	a
DEKL^{++}	38.10	23.78	Dekelia; air base, 1 story	175°$^{*+}$	4	c
DMKA^{+}	37.99	23.82	Ag. Paraskevi; research centre, 1-story RC	135°	4	b
FIXA^{+}	37.96	23.73	Sygrou-Fix; metro station, −15 m	140°	4	c
PEFK**	38.08	23.62	Thriassion plain; warehouse, 1 story	0°	6	c
RNTA^{++}	37.96	23.68	Rentis; town hall, 2-story RC	210°	4	c
SGMA^{+}	37.98	23.74	Syntagma; metro station, −7 m	010°	7	b
SGMB^{+}	37.98	23.74	Syntagma; metro station, −26 m	135°	3	b
SPLA^{+}	38.00	23.71	Sepolia; metro station, −13 m	320°	18	c
SPLB^{+}	38.00	23.71	Sepolia; metro station, 3-story steel	320°	19	c
FILI**	38.12	23.68	Fili Monastery; free field	0°$^{!}$	6	b
THVC^{+}	38.32	23.32	Thiva; town hall, 3-story RC	180°	5	b
PSAR**	38.09	23.56	Goritsa; house, ground floor, RC	0°	6	c
MAGO**	38.08	23.52	Magoula; 1-story RC	0°$^{!}$	6	a
STEF** N00E bad	38.17	23.55	Stefani; storage, ground floor, RC	0°$^{!}$	5	b
ZOFR**	38.07	23.69	Zofria; free field	0°	6	a
NEOK**	38.05	23.63	Neokista; ground floor, RC	0°$^{!}$	6	a

$^{+}$NOAGI station.
$^{++}$NOAGI; did not record main event.
**University of Athens data; did not record main event.
$^{*+}$.t component −90.0 from .l component.
$^{!}$Polarity may be reversed.
Underlined stations are used in the source parameter inversion.

although it crosses the mesoseismal area at a shallow depth. No damage was reported to the new underground metropolitan railway. The Mornos aqueduct, which supplies Athens, suffered no damage, although it runs almost parallel to the Aspropyrgos Fault and through the mesoseismal area.

Main shock data

Fifteen strong-motion accelerograph stations recorded the main shock near and around Athens. Ioannidou *et al.* (2001) describes the main shock records and aftershock recordings used to obtain the EGFs. The peak ground accelerations ranged from 0.05 to 0.5 g. The National Observatory of Athens Institute of Geodynamics (NOAIG) recorded data with its permanent strong-motion array and Attico Metro S. A. instruments. The NOAIG procedure for processing strong-motion records is based on the standard procedure used at the California Institute of Technology (Trifunac & Lee 1973) and is described by Stavrakakis *et al.* (1993). For this study, we synthesized observed records at ATHA, DMKA, FIXA, THVC, SGMA and SPLA. Two available sites were not used: SGMB, which is located just 19 m below SGMA, and SPLB, which is at the same depth and geology as SPLA but is 150 m distant. SPLB is in the basement of a three-story steel structure. These eight are the only sites that recorded the small earthquakes needed for the EGFs.

Table 2 lists source parameters of the main Athens earthquake reported by several institutions. Estimated epicentral locations were fairly well constrained (excluding Harvard's), but depths ranged from approximately 8 to 17 km. Focal mechanism solutions are in overall agreement, corresponding to an extensional WNW–ESE-trending nodal plane dipping SW. Papadopoulos *et al.* (2000) interpreted the aftershock distribution as a zone striking WNW–ESE with a length of 25 to 30 km, dipping 80° SW. However, the variations in focal parameters and locations and the absence of surface trace do not permit association with a particular fault. No surface rupture was apparent. Secondary gravitational fissures, small ground cracks, minor landslides, and falling rocks have been mapped near

Table 2. Source parameters for main event.

Latitude	Longitude	Depth (km)	Moment (10^{24} dyne-cm)	Duration (s)	Focal mechanism (STK DP SV)	Institution/ Reference*
38.08	23.58	16.8			113° 39° −90°	NOAIG^{+}
38.105	23.565	8	17.0	5	105° 55° −80°	ATHU
38.132	23.545	10	7.8		123° 55° −84°	USGS
38.119	23.605	10				PDE
37.87	23.64	15	11.0		116° 39° −81°	Harvard
			11.22			This study

$^{+}$Papaddopoulos *et al.* (personal communication, 2000).

the village of Fili (Fig. 2), consistent with active features striking N 120°–130° and dipping 70°–80° SW with a rake angle of −76° to 88° (Pavlides *et al.* 2002). Using teleseismic inversion of body waves, Papadimitriou *et al.* (2000) and Louvari & Kyrazti (1999) estimated the depth of the main event at 8 and 11 km, respectively, with a source duration of about 5 s. Most of the energy was released in the first few seconds. Detailed seismological information about the earthquake can be found in Stavrakakis (1999).

Weak motion data

The University of Athens Department of Geophysics and Geothermics (UoADGG) deployed two types of stations as a temporary network to record aftershocks. These sites were primarily in the area of high damage, but none was located where the main event was recorded. Acceleration was recorded at sites PEFK and COUR, situated within the centre of the network, using Kinemetrics ETNA instruments. The previously mentioned procedure for processing strong-motion accelerometer records was applied on the data from these stations. At the NEOK, STEF, MAGO, FILI, PSAR and ZOFR sites, RefTek recording instruments were installed. The first four of these were equipped with the LE-3D 1-Hz Lennartz sensor, while the last two stations were connected to GURALP CMG 40-T broadband seismometers. Data were instrument-response-corrected according to the sensor specifications of obtained velocity time histories and were differentiated to provide accelerograms.

Geology and site conditions

Fig. 3 shows the geology of the study area, and Table 1 describes the geologic conditions at the recording sites, as discussed in Ioannidou *et al.* (2001). In Table 1, (a) indicates the hard rock formations of dolomites or limestone of U. Triassic to L. Jurassic age and limestone of U. Cretaceous age; (b) indicates rock and soft rock formations of slightly to medium-weathered phases of the Athens Schist, metamorphosed schist and limestone, cohesive talus cones, and medium- to well-cemented conglomerates or Neogene marls; and (c) indicates soil and stiff soil formations of moderately thick weathering products of the geologic bedrock, alluvium deposits of medium to high density or recent man-made deposits. The sites are composed primarily of shales, sandstones and crystalline limestones, and soil conditions range from firm soil to alluvium. Most of the recording sites are in the vicinity of major infrastructure that was either constructed in the past or under construction at the time of the earthquake, such as the surface or underground stations of the Athens Subway (DFNA, FIXA, PNTA, SGMA, SGMB, SPLA and SPLB). The records used in this study ranged from 0.05 to 0.2 g for all stations except SPLA, which had 0.3 g, and are not considered to be in the non-linear response range. Station SPLA is on competent soil and may have had non-linear response; however, the observation that its records are modelled as well as those at other stations suggests that it did not.

Empirical Green's functions

In this study, we modelled ground motion with empirical Green's functions for frequencies between 1.0 and 20.0 Hz. Most of the events we used have moments greater than the threshold identified by Hutchings & Wu (1990) for effectively impulsive point sources. To create EGFs, we used the output of a source parameter study to deconvolve out the finite Brune source from the recordings. We confine this approach to events with magnitude <4.0 to minimize significant finite source effects and keep the basic assumption of the Brune source model. This constraint extends the synthesis methodology of Hutchings & Wu (1990) to include events larger than those that satisfy the criteria for effectively impulsive point shear source earthquakes.

Empirical Green's functions cannot be recorded with the same focal mechanism solution from all locations along a fault of interest. Therefore, we interpolated EGF source locations and focal

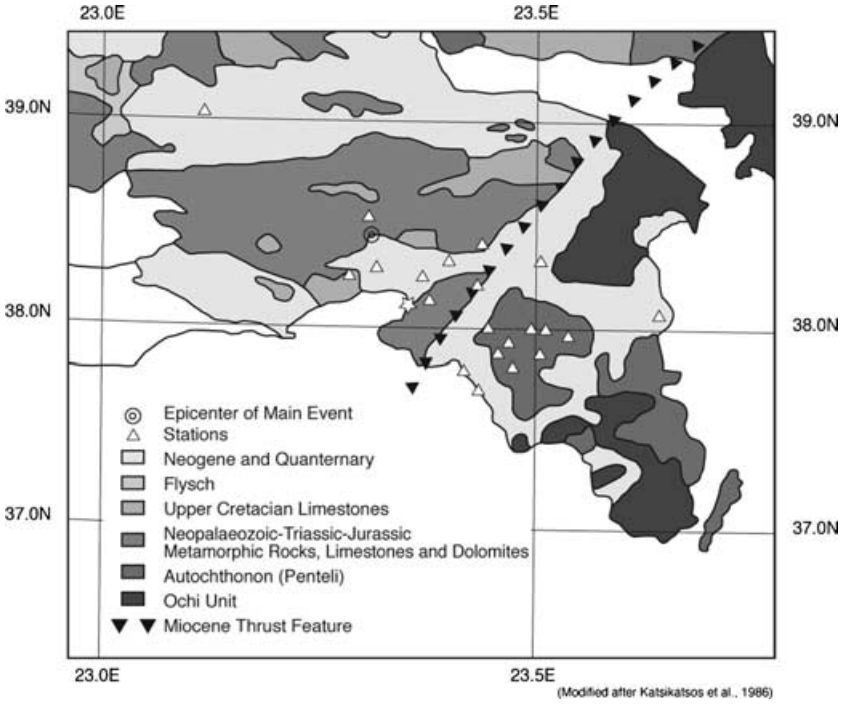

Figure 3. Geology of the lower border area of Attica (modified from Katsikatsos *et al.* 1986), station locations, and epicentre of main event.

Table 3. Source parameters of events.

Earthquake Date and Time	Latitude (°N)	Longitude (°E)	Depth (km)	$M_w^{!!}$ (M_L)$^!$	M_o (10^{20})	f_c	SD	Mechanism (STK DP SV)	No. of stat.
1999/09/07 11:56:51*	38.08	23.58	16.8	6.0 (5.4)	112,200	0.45		113°39°−90°*	10
1999/09/07 11:59:10$^+$	38.15	23.59	5.0**	4.2	218	3.2	212		6
1999/09/07 12:00:29$^+$	37.92	23.78	17.8	4.3	277	3.2	142		6
1999/09/07 12:01:57$^+$	38.07	23.75	5.0**	3.7	30.4	2.4	14		2
1999/09/07 12:03:54$^+$	38.01	23.47	5.2	3.6 (3.5)	30.0	6.4			1
1999/09/07 12:05:12$^+$	38.11	23.69	5.0**	4.3	197	2.7	127		4
1999/09/07 12:08:11$^+$	37.82	23.71	5.0**	4.3	222	3.5	286		4
1999/09/07 12:16:10$^+$	37.96	23.76	17.0	4.4	380	3.4	247		4
1999/09/07 12:20:25$^+$	38.09	23.65	5.0**	4.2	218	5.1			1
1999/09/07 13:02:02$^+$	38.07	23.62	5.0	3.7	20.7	3.5	27		2
1999/09/07 13:05:48$^+$	38.13	23.51	18.2	4.2	325	3.1			1
1999/09/07 15:35:33*$^+$	38.01	23.48	10.0	4.1(3.9)	106	4.2	188		6
1999/09/07 15:42:52*$^+$	38.07	23.45	3.0	3.6 (3.5)	26.6	7.5			1
1999/09/07 17:19:21*	38.11	23.72	16.2	4.1(3.8)	90.8	7.0	547	114° 30° −87°	4
1999/09/07 20:44:55*	38.19	23.72	21.0	5.0(4.4)	3212	0.9	28		3
1999/09/08 03:21:32*	38.09	23.83	14.1	4.1(3.7)	92.3	4.2	136		7
1999/09/08 03:35:20*	38.12	23.89	13.0	4.1(3.7)	195	7.4	1636	106° 30° −74°	3
1999/09/08 11:14:29*$^+$	37.99	23.59	7.0	3.9(3.1)	29.5	2.9	21		2
1999/09/08 12:55:01*	38.14	23.74	19.9	4.1 (4.0)	134	2.9	61	330° 70° −30°	2
1999/09/08 13:18:21*	38.08	23.81	9.2	3.8(3.7)	27.1	3.6	44		4
1999/09/08 16:50:37*	38.19	23.91	1.4	3.8 (3.6)	48.5	4.0		113° 28° −67°	1
1999/09/08 16:54:08*	38.14	23.79	19.4	3.9 (3.5)	84.7	4.1		310° 50° −20°	1
1999/09/10 14:49:57^{++}	38.08	23.67	9.1	4.0(3.7)	85.5	5.4	326	319° 70° −79°	10
1999/09/13 19:45:15^{++}	38.06	23.65	9.1	3.7(3.1)	15.4	5.3	57	109°50° −74°	10
1999/09/16 08:12:10^{++}	38.06	23.66	7.9	3.7(3.1)	17.6	4.9	56	120° 54° −89°	10
1999/09/20 19:58:09*$^+$	37.96	23.53	7.0	3.4(2.9)	7.29	6.9	67		9
1999/09/20 20:17:25^{++}	37.97	23.64	8.8	2.9(2.9)	1.36	6.6	10	250° 65° −48°	7
1999/10/03 17:03:34^{++}	38.09	23.75	9.0	4.0(3.5)	75.7	3.6	91	159° 65° −48°	9
2000/03/23 03:09:18*$^+$	38.08	23.74	15.0	4.1(3.5)	148	4.2	202	120° 54° −89°	4

*Location from Papadopoulos *et al.* (2000).
$^+$Location obtained from permanent networks in Greece and *S*- and *P*-wave arrival-time intervals.
$^{++}$Solution from combined data of University of Athens and National Observatory of Athens.
*$^+$Locations routinely calculated by NOAIG from their permanent Greek network.
**Depth fixed.
$^{!!}$Magnitude obtained from moment/magnitude relationship in Hanks & Kanamori (1979).
$^!$Local Richter magnitude obtained from UoADGG.
***Moment and magnitude obtained from spectral overlay with event 1999/09/07 15:42:52.
M_0 and f_c determined by stations indicated in Table 1.

mechanism solution to fill in the fault. Interpolation for location is performed by correcting for attenuation, geometric spreading, and *P*- and *S*-wave arrival times due to differences in source distances, as discussed in Hutchings & Wu (1990). We interpolated for focal mechanism solution by modifying *P*- and *S*-wave radiation pattern coefficients determined from focal mechanism solutions if available. However, Hutchings & Wu (1990) and Jarpe & Kasameyer (1996) found that, for high frequencies, focal mechanism interpolation does not improve the synthesis.

In this study, source events for EGFs are distributed throughout the area and do not necessarily occur on the fault being modelled. In this application, the EGFs carry the average propagation properties of the area and a site-specific site response. In studying the spatial dependence of EGFs, Hutchings & Wu (1990) found that differences in source location and/or focal mechanism solutions cause much less ground-motion variability than site response. Hutchings & Wu (1990) and Steidl (1996) showed that the primary variability in structure occurs near the surface; thus, a recording site captures the variability near that site. This correspondence is apparent in results of the syntheses below, which show that the site-specific characteristics of the observed accelerograms are well matched.

Source parameters of aftershocks

We used the computer program NetMoment to estimate critical source parameters of the aftershocks that provided EGFs. NetMoment conducts a simultaneous inversion of aftershock recordings to obtain source moment (M_0) and corner frequency (f_c), and site-specific kappa (κ) (Hutchings 2004). Details of the approach are described in Ioannidou *et al.* (2001) and Gok & Hutchings (2006). This study is similar to that presented in Ioannidou *et al.* However, we incorporated whole-path κ with site-specific κ in the calculations, and we only used stations without a significant site response in the inversion. Stations from the Ioannidou *et al.* study that did not have a significant site response are underlined in column one of Table 1. The simultaneous inversion is based upon the assumption that for a particular earthquake, moment and source corner frequency will have the same value when calculated from spectra at each site; therefore, differences in spectra are due to site response, propagation path κ, and individual site κ. There is often a trade-off between κ and source corner frequency. Gok & Hutchings (2006) found that the simultaneous solution approach provides stable results which have been validated by independent studies. The error ellipse

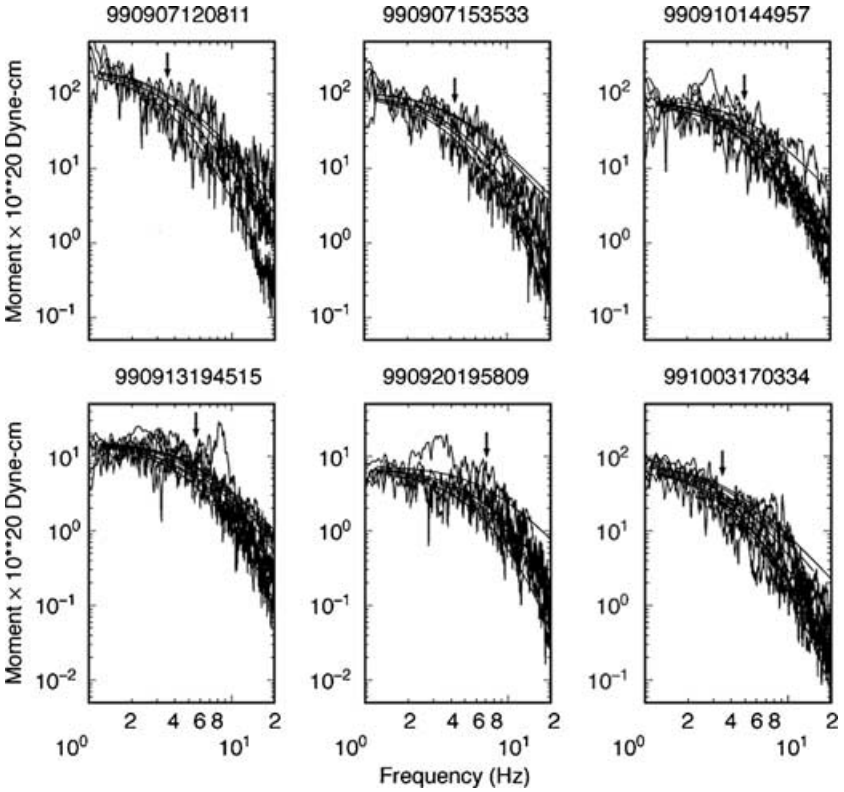

Figure 4. The observed spectra and the fit to calculated Brune spectra by varying moment, source corner frequency and site-specific κ. The arrow shows the source corner frequency calculated.

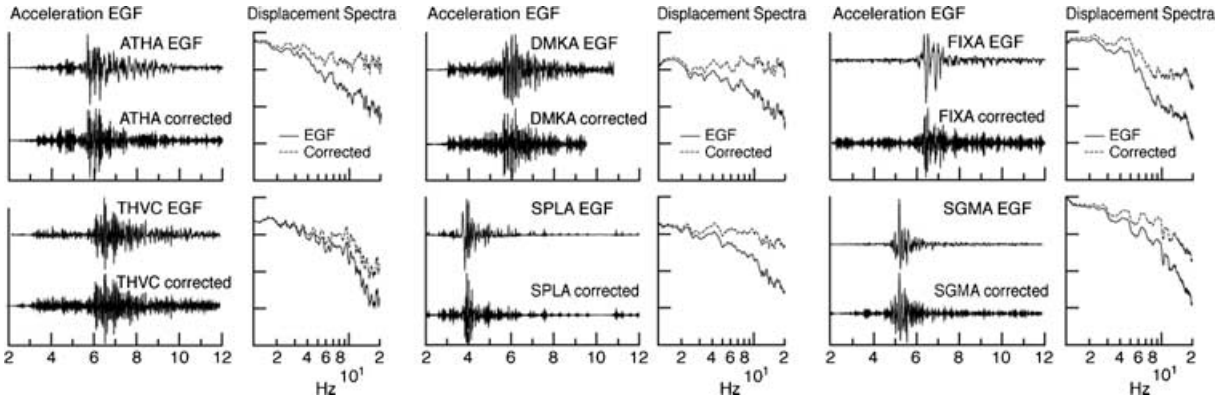

Figure 5. Recorded seismograms and spectra (identified by EGF) and results after the Brune source model has been deconvolved (identified by 'corrected').

for the 98 per cent confidence level ranged from ± 0.05 for κ and ± 25 per cent for f_c for most events.

Table 3 lists the source parameters determined and the number of aftershocks used in the inversion. Fig. 4 shows fits to observed spectra for several events and the corner frequency calculated (arrow). The differences in shapes of individual spectra are due to site-specific κ. The solid line shows the modified Brune model over the frequency band used. The actual moment is the projection of this fit to DC frequency. Data have been normalized to have the same long period spectral levels as described in Ioannidou *et al.* (2001) and Gok *et al.* (2006).

Effectively impulsive point sources

Deconvolution with a Brune source assumes that the event is essentially a point source with finite time duration. Removing the Brune spectral shape to create flat displacement spectra creates effectively impulsive point source events. The Brune source has zero phase shifts so that in the deconvolution only the amplitude spectra are affected, and there is no non-causal effect in the time-series. Fig. 5 shows several recordings that have been deconvolved to provide effectively impulsive point shear source event recordings (EGFs). The time-series are in acceleration, and their displacement spectra

are shown. The observation that the spectra are not flat after the deconvolution is assumed to be due to effects of attenuation and site response (f_{max} effect) and uncertainty in the corner frequency solution obtained.

Fault rupture model constraints

Here, we estimate boundaries for the possible rupture parameters that may have been identified prior to the 1999 earthquake. Rupture parameters are randomly varied by the HAZARD program to create scenario earthquakes as discussed above.

Moment. The moments listed in Table 2 show an approximate factor of 2 variation in estimates for the 1999 earthquake, from 7.8 dyne-cm to 17.0 $\times$ 10^{24} dyne-cm. The resulting moment magnitudes range from 5.9 to 6.1 dyne-cm, respectively. The average of moments from Table 3 is 1.19 $\times$ 10^{25} dyne-cm. For this paper, we use 1.122 $\times$ 10^{25} dyne-cm, which gives a moment magnitude of 6.0, using the Hanks & Kanamori (1979) relation.

Fault rupture geometry. Fault shapes are constrained to be elliptical. For this study, the length of the major axis is constrained to vary from 7 to 13 km, and the eccentricity varies from 0 to 0.90, which limits the minor axis to be between about 5 and 11 km. With these constraints, the fault area ranges from about 40 to 110 km^2, with an average area of 90.6 km^2. Wells & Coppersmith (1994) obtained an area of 93 km^2 for the $M_w = 6.0$ earthquake by regression of all earthquakes in their data set, and Somerville *et al.* (1999) obtained 79.9 km^2.

Hypocenter. The hypocenters are only confined by the description above. Scenario earthquake rupture areas must fall between 0 and 25.0 km to keep them within the brittle crust. However, no surface rupture is allowed. No quaternary surface faulting has been observed in the geologic record for the area.

Strike. The Kifissos and Aegaleo fault zones in the eastern part of the selected area trend NE–SW, while the Thriassion fault zone to the centre and west of the epicentral area trends WNW–ESE. In the western part of the latter zone, W–E faults are also apparent, coinciding with the extensional faults of the seismically active, major graben structure in the Corinthian gulf further west. The morphological expression of the Thriassion Pedion Fault can be identified in aerial photographs and satellite images. North of the Thriassion Pedion Fault, smaller faults with similar strike direction span the block of Parnitha Mountain. Because of this faulting and the uncertainties of strike at depth, we limit the strike of possible rupture to be between N100°E and N125°E.

Slip vector. The extension character in the area is prominent, leading us to limit the rupture to normal or oblique slip, although the kinematic complexity of the structures indicates that reverse or thrust faults were almost certainly present in the past (Mariolakos & Foundoulis 2000). We limit the slip vector to be from −70° to −110°. However, the slip vector values are used only when the EGFs have a focal mechanism solution. If no focal mechanism solution is available, we use an average of 0.63 for the *S*-wave correction factor.

Dip. The dip is limited to range from 35.0° to 55.0°, following the same argument as the slip vector.

Slip distribution. Slip amplitude values, with or without asperities, are allowed to vary between 10 and 100 cm. The average slip amplitude ranged between 28 and 56 cm. Our slip models had an average of 20 per cent with slip greater then 1.5 times average slip and ranges from 10 to 40 per cent.

Stress drop. Orowan stress drop varies between 3 and 350 bars, with a median of 30 and an average of 50 bars.

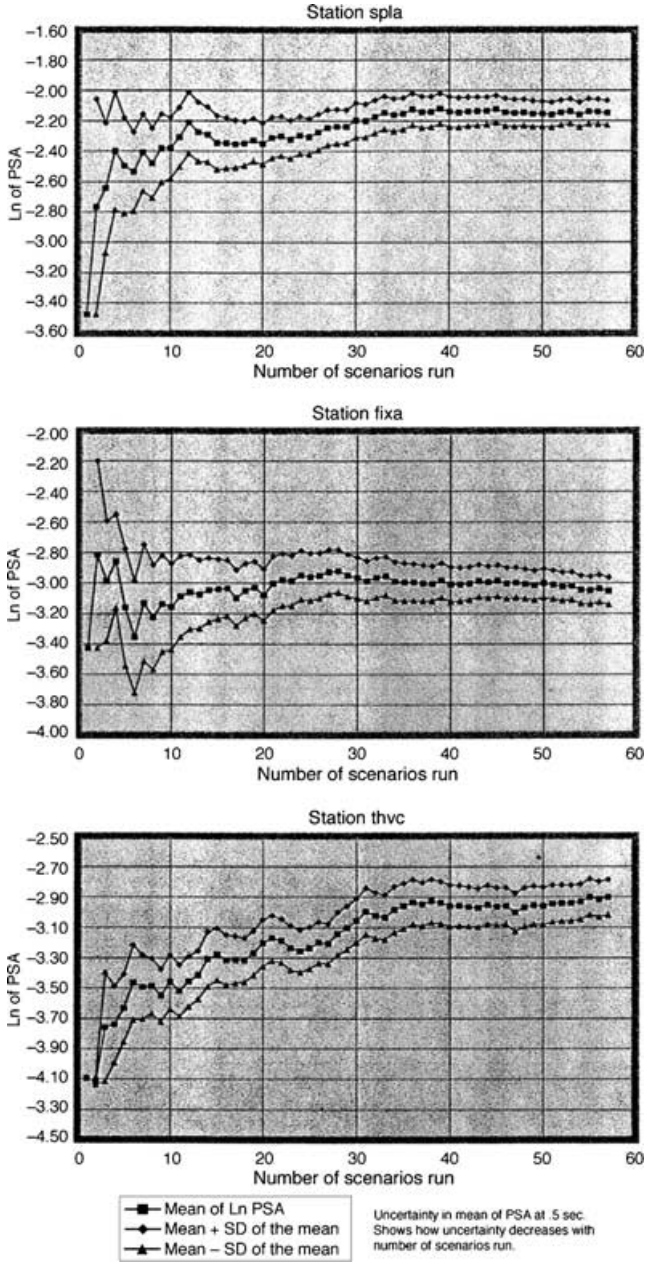

Figure 6. The mean of the absolute acceleration response at a 0.5-s period as a function of the number of scenarios run (centre line), and the one standard deviation of the estimates of the mean. The mean stabilizes after about 40 scenarios.

Source volume for 1999 main shock. No specific fault was identified prior to the 1999 event, but several studies could have limited the possible rupture surface to be within a small source volume near Athens (Fig. 2). The range of hypocenters for the 1999 earthquake occurred in the volume (Table 2). Papadimitriou *et al.* (2000) interpreted Aegaleo Mountain as acting as a barrier to rupture. Tselentis & Zahradnik (2000) discussed a fault surface determined by the distribution of aftershocks occurring during an 11-day period at depths of 3.5 to 15.5 km, which coincides with the fault plane computed by the U.S. Geological Survey (USGS). The absence of aftershocks in an 8-km by 10-km area is interpreted as the area ruptured by the main event. EGF waveform modelling by the same researchers allows for a larger area ruptured by the main event. In addition, interferograms

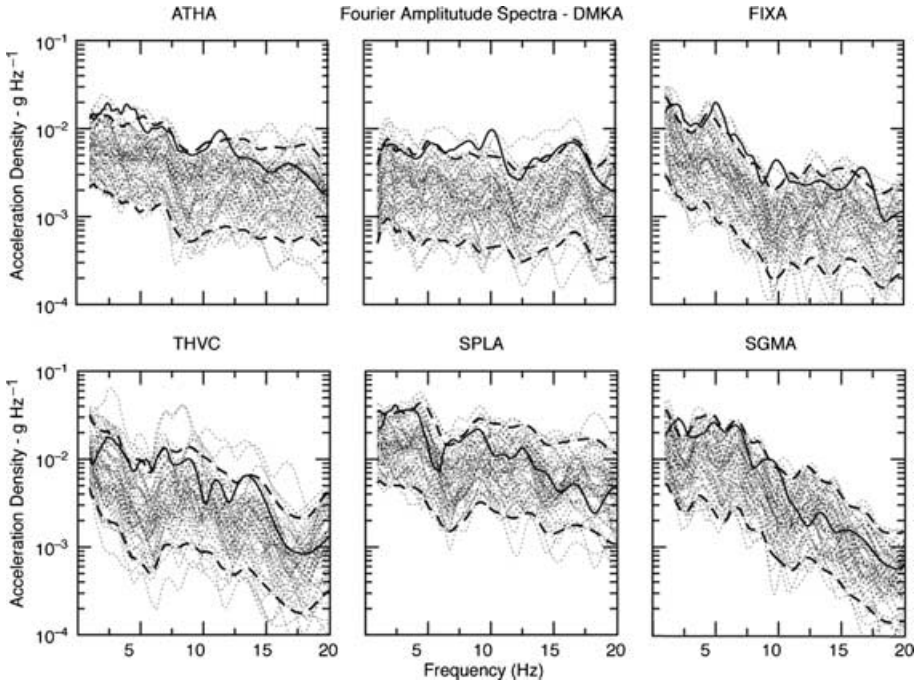

Figure 7. Fourier amplitude spectra for each of the 57 scenarios (dotted line) in the smaller source volume where the Athens earthquake is thought to have occurred; the plus-and-minus standard deviation values of the prediction (thick dashed lines); and the AAR recorded (thick solid line).

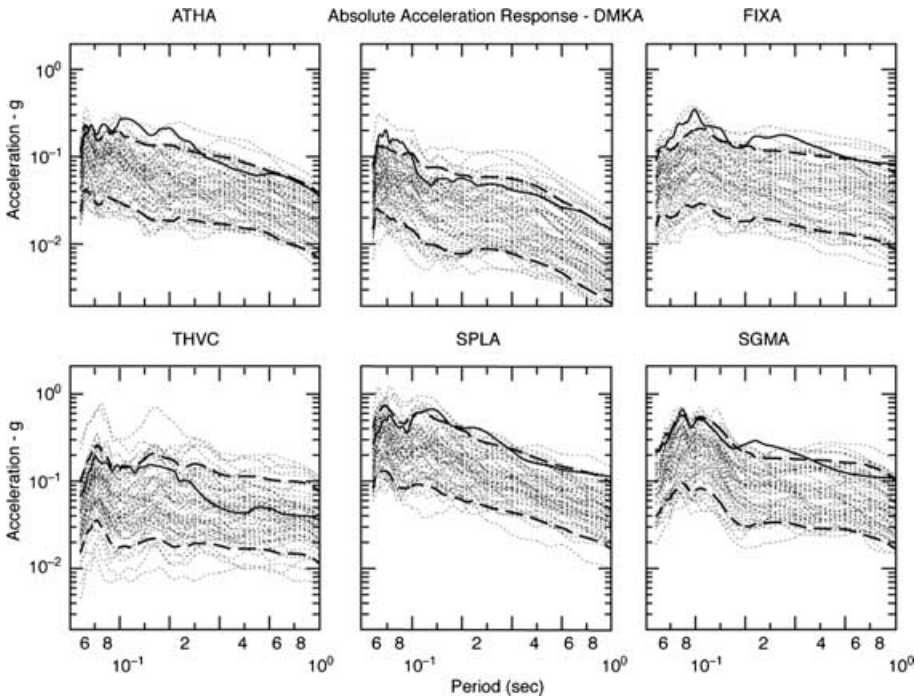

Figure 8. Absolute acceleration response calculated for each of the 57 scenarios (dotted line) in the smaller source volume where the Athens earthquake is thought to have occurred; the plus-and-minus standard deviation values of the prediction (thick dashed lines); and the actual AAR recorded (thick solid line).

(Kontoes *et al.* 2000) present a deformed area of 20 km E–W by 10 km N–S. No fringes extend beyond the Aegaleo Mountain, but they do extend to the east, north of the mountain. With these studies, we confined the volume for the rupture of the 1999 earthquake to be between 38.00° and 38.14°N, 23.53° and 23.67°E, and 0 to 25.0 km in depth. Therefore, a 12.3-km × 15.3-km × 25.0-km volume contains the entire rupture of the scenario events.

Source volume for $M_w = 6.0$ *earthquakes*. We interpreted the larger source-zone volume within which $M_w = 6.0$ earthquakes could occur near Athens from the neotectonics of the greater Attica area. Although Athens has been affected by stronger, more distant events, $M_w = 6.0$ are the largest considered likely to occur near the Athens metropolitan area. Neotectonic faults capable of causing an event this size consist of a complex post-alpine structure, which is

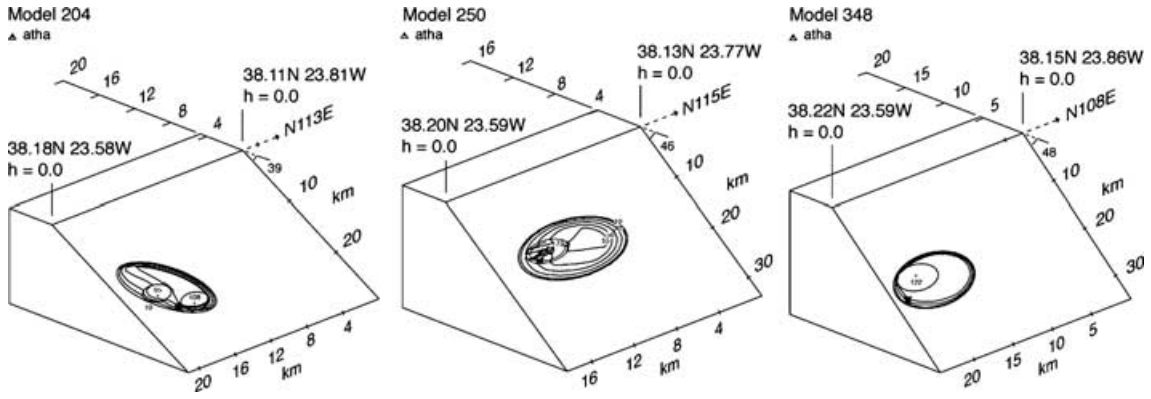

Figure 9. The rupture models for scenarios that provided the best fit to observed seismograms. Model ATH204 is the preferred model.

characterized by complicated kinematic and dynamic evolution and involves major fault blocks with different rotational axes trending NE–SW and E–W. The geologic structure consists primarily of the tectonic graben of the Thriassion plain and the complex neotectonic graben of the West Athens basin, the mountains of Parnitha and Aegaleo belonging to the Mesozoic non-metamorphic eastern Greece unit, and the Pendeli and Ymittos mountains belonging to the Mesozoic metamorphic unit (Fig. 3). The tectonic contact of these units is interpreted to be in the NE–SW direction, and its location coincides with the Kifissos River (Mariolakos & Foundoulis 2000); this position roughly coincides with the Miocene thrust feature shown in Fig. 3.

We confined the rupture area of any likely $M_w = 6.0$ earthquake to be between 38°00′ and 38°15′N and between 23°25′ and 23°40′E, and a depth of 0 to 25 km. Therefore, the morphological features of the Aegaleo Mountain to the southeast and the Kifissos River to the northeast define the extension of the proposed rupture area to the east. Additionally, the proposed rupture area extends N–S to include most of the Parnitha Mountain area. It is defined to the south by the Thriassion fault zone and to the north by the change in the geologic border between the Neopalaeozoic–Triassic–Jurassic metamorphic rock unit and the Neogene and Quaternary unit (Fig. 3).

RESULTS

Strong ground-motion prediction

One purpose of our study was to predict the range of ground motion that may occur from an earthquake at a particular magnitude within a source zone or along a fault. We used the program HazStats to predict the range of ground motions that might have been identified prior to the 1999 earthquake. Fifty-seven models from the larger set of 500 (discussed below) fell within the possible source volume for the 1999 event, and we used them to test our prediction hypothesis. First, we examined whether we ran enough scenarios to capture the variability of ground motion. Fig. 6 shows the mean of the absolute acceleration response at a 0.5-s period as a function of the number of scenarios run. After about 40 scenarios, the mean stabilizes, indicating that our 57 models span the full variability of ground motion possible from this approach.

We then calculated the median (lognormal mean) plus one-standard-deviation values of linear ground motion at sites ATHA, DMKA, FIXA, THVC, SGMA and SPLA and compared these to recorded values. The one-standard-deviation values also include an error for uncertainties in the methodology, as discussed above. These are the only stations that recorded the main event and aftershocks at distinctly different sites. Stations SGMB and SPLB also recorded the main event and aftershocks, but they were too closely located to SGMA and SPLA to add to the test.

Fig. 7 shows the Fourier amplitude spectra for each scenario (dotted lines), the plus-and-minus standard deviation values of the prediction (thick dashed lines), and the actual Fourier amplitude spectra recorded (thick solid line). Fig. 8 shows the same plots for the absolute acceleration response (AAR). The recorded data are at or just below the one-standard-deviation value of the synthesized suite of spectra. The one-standard-deviation values represent the 84th percentile in the prediction.

We conclude that the shapes of the spectra in general match the shapes of the observed spectra; that with the epistemic and aleatory uncertainties assumed, the observed spectra fall within or very close to the one-standard-deviation values; and that we demonstrate the prediction capability. Several validation exercises similar to this one will be needed to determine whether the methodology is validated.

Rupture model of the 1999 earthquake

Another goal of our study was to identify the most likely rupture scenario for the 1999 Athens earthquake. To identify the best rupture models, we calculated the goodness of fit between observed and synthesized records using the method developed by Anderson (2003). We used the program COMPARE to make this calculation. Anderson suggests calculating the fit of ten parameters: Arias duration, energy duration, Arias intensity, energy integral, peak acceleration, peak velocity, peak displacement, absolute acceleration response, Fourier spectra, and cross-correlation. Arias intensity and energy integral are proportional to the integral of the acceleration and velocity squared, respectively. The Arias and energy durations are defined as these integrals normalized by their maximum value, and the goodness of fit is determined by one minus the maximum of the difference between the observed and calculated normalized integrals. Each estimate is given a value of 0 to 10, so that the final score is between 0 and 100, with the latter being a perfect fit. Anderson finds that 40 to 60 represents a fair fit, 60 to 80 a good fit, and 80 to 100 an excellent fit. We averaged all estimates for goodness of fit over their values at frequency bands 1–2, 2–5, 5–10, 10–20 and 1–20 Hz as suggested by Anderson (personal communication, September 2004), except Fourier and absolute acceleration response, which are calculated for each at frequency band 1–20 Hz only and averaged. We averaged the values obtained from three components and further averaged the values obtained at all six sites,

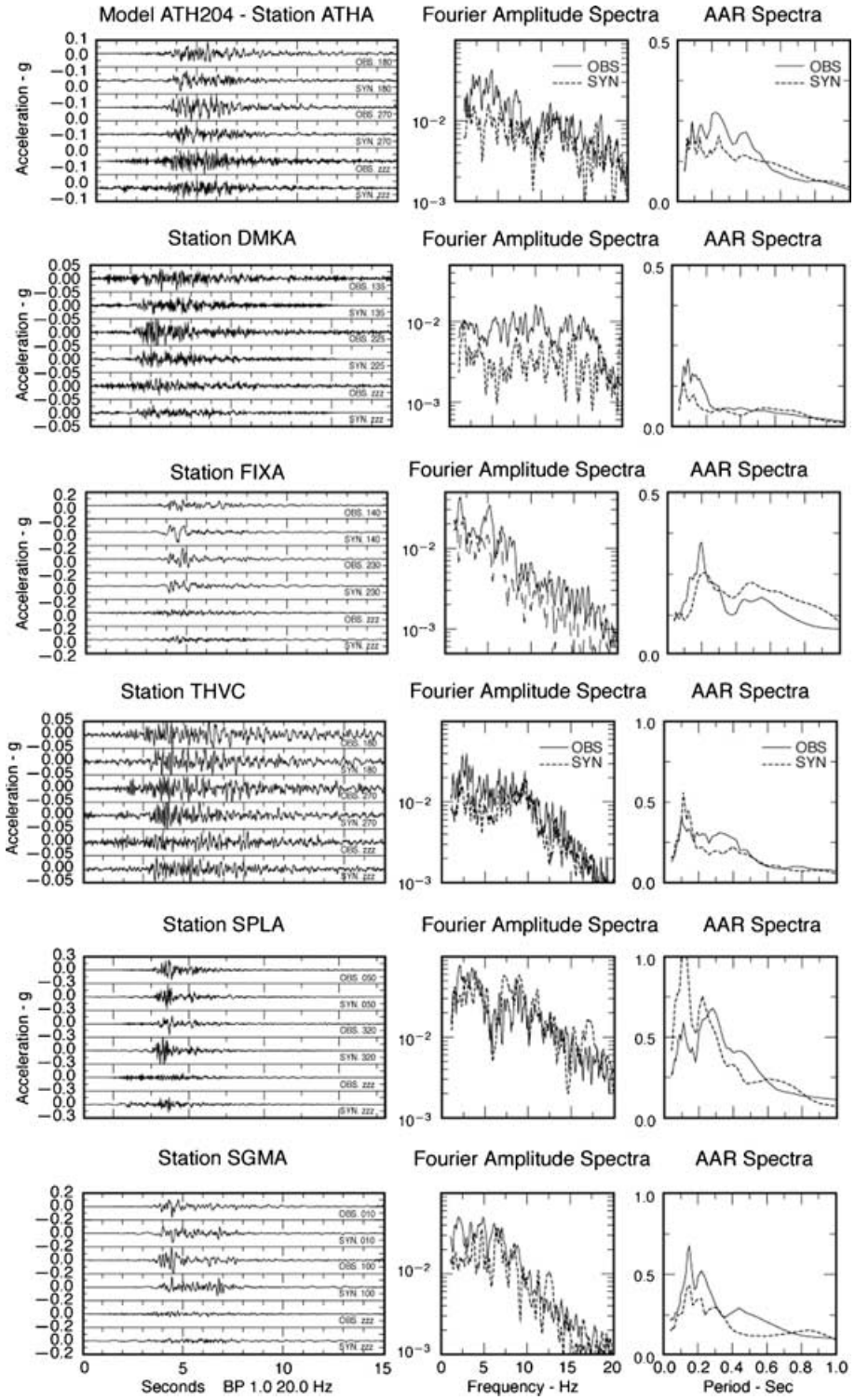

Figure 10. The fit to seismograms for all stations in the study for rupture model ATH204. Notice that the basic characteristics of the synthesized seismograms (SYN) closely match the observed seismograms (OBS). In particular, the basic waveforms, durations and frequency content match well. The frequency content is evident from the Fourier amplitude and ARR spectra. The solid lines are observed spectra and dashed lines are synthesized spectra.

which gave us a final score that represents how well a rupture model generates the observed accelerograms.

Values for the 57 models ranged from 20 to 67. Three models (Fig. 9) had the best rating of fits to observed seismograms (models M204, M250 and M348, with ratings of 67, 61 and 64, respectively). The three models had similar rupture patterns and occurred in the vicinity of 38.05°N, 23.60°W, with the centre of rupture near 12 km and nearly unilateral rupture toward Athens. Strikes ranged from N107°E to N115°E, dips ranged from 39° to 48°, rupture velocity ranged from 0.92 to 0.99 times V_s, and healing velocity ranged from

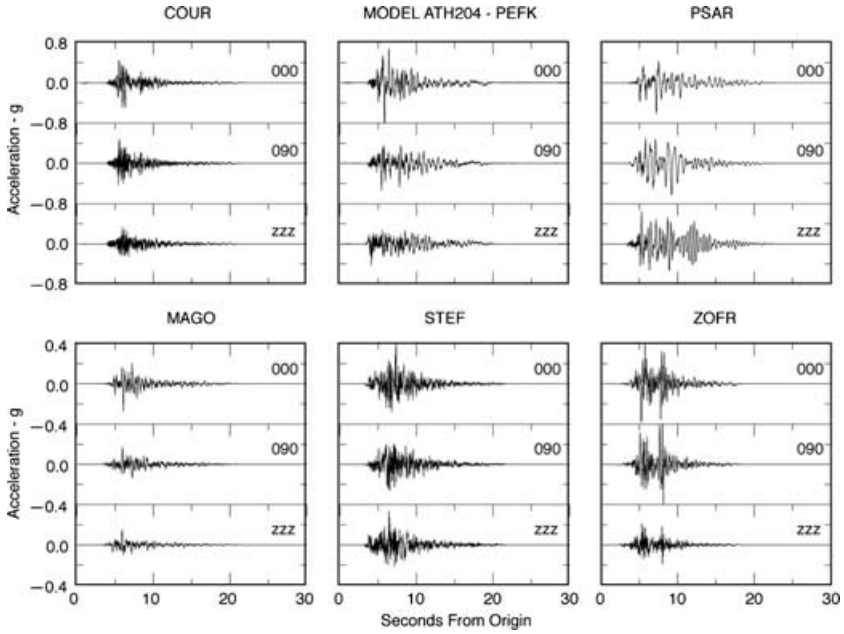

Figure 11. Synthesized seismograms at stations that did not record the main event but were in locations where high damage occurred.

0.89 to 0.95 times V_r. Although the rupture models are very similar, the fit to observed seismograms is better at some stations than at others. However, those from model M204 generated the best seismograms by the Anderson method and by visual inspection. Fig. 10 shows the fit to recorded seismograms for this model. The fit to seismograms indicates that, for engineering purposes, this methodology can provide realistic ground motion in advance of an earthquake.

As Fig. 10 shows, in general, the shape of the spectra and character of the time-series match well at each station with the exception of the Fourier amplitude spectra at station DMKA. At other stations, there is some misfit over short frequency intervals. However, the choice of a 'match' is based upon the 'score' from the Anderson comparison method of 10 parameters over five frequency bands. Also, notice that the spectral shapes and character of the seismograms are considerably different at each site. The site-specific character of these factors is controlled by the EGFs and the geometric relationship to the source rupture. It is interesting to compare Fig. 5 with Fig. 10. Fig. 5 shows the basic character of the EGF at each site when only the propagation path and site effects are included. Fig. 10 shows the resulting seismograms when they are convolved with the rupture model of the main event. The basic character of the high-frequency spectral shapes is the same.

Our assumption is that if accelerograms give a good fit to observed records, then the rupture model is closely simulating the actual fault rupture. This assumption seems fair, given that the fit is made to low and high frequency, acceleration, velocity and displacement and the 'true' Green's functions are used. One can imagine that an even better fitting model could be found by iterating around the rupture parameters of models M204, M250 and M348. We ran HAZARD for 25 models with parameters close to these models but did not find a better fitting set of synthesized seismograms on average. We also ran 20 models with small variations around model M204. We kept the fault geometry and hypocenter the same but varied the rupture and healing velocity, roughness and asperities. This calculation did not result in significant improvement. We conclude, from our basic assumption, that the actual Athens earthquake had a rupture similar to those of models M204, M250 and M348. Also, our 'best' fitting model is near the limit of what we can achieve by modelling exact rupture and fitting seismograms with this methodology.

Our 'best' rupture models agree with previous studies. Tselentis & Zahradnik (2000) modelled the rupture of the main event with EGFs using Irikura's synthesis approach at one station more than 200 km away. Their results showed a similar fault size, orientation and location as our study. Roumelioti *et al.* (2003) also modelled the Athens earthquake with an EGF method (different from this paper or Irikura's method) at nine regional stations greater than 200 km away and found a slip distribution and strong unilateral rupture similar to this study. Roumelioti *et al.* (2004) used this rupture model to model the Athens earthquake with a stochastic method for finite faults.

Extrapolation of ground motion

To simulate ground motion in areas where the main earthquake was not recorded, we used the rupture scenario ATH204 and modelled accelerograms at stations COUR, PEFK, PSAR, MAGO, ZOFR and NEOK. (We did not use the STEF accelerogram because it had a bad horizontal component.) The reader is referred to Ioannidou *et al.* (2001) for detailed information on the geology and site response of these sites and others referred to in this paper. Fig. 11 shows the synthesized seismograms at these stations. In general, station MAGO had significant accelerations in the 0.2-g range; stations COUR, ZOFR and NEOK had significant accelerations in the 0.3- to 0.4-g range; and stations PEFK and PSAR had significant accelerations in the 0.4- to 0.8-g range. These accelerations are consistent with the intensities documented for the earthquake. Stations ZOFR and COUR are in the intensity VIII zone, and stations PEFK, PSAR, MAGO and NEOK had intensities in the VII zone (Fig. 2). Station SPLA, which recorded the main event (Fig. 10), is also in the intensity VII zone and had accelerations in the 0.3-g range. Except for MAGO, these sites had accelerations greater than the other actual recorded strong motions, which ranged from 0.04 to 0.2 g. According to Ioannidou *et al.* (2001), station MAGO showed

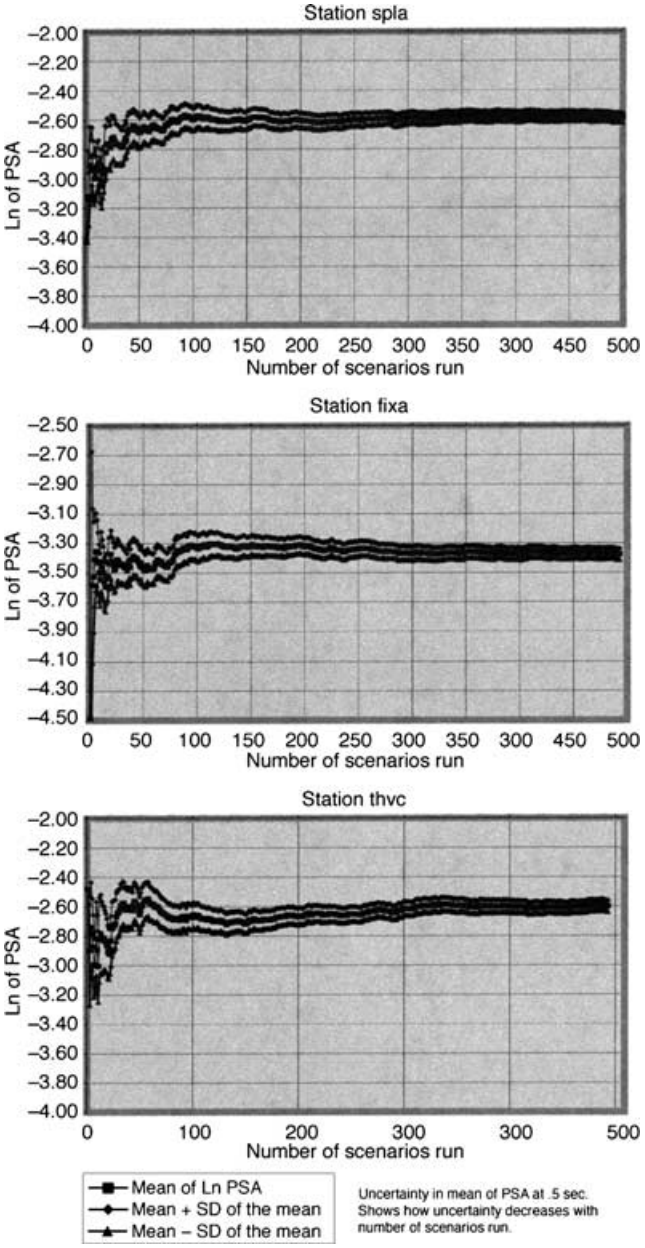

Figure 12. The mean of the absolute acceleration response at a 0.5-s period as a function of the number of scenarios run (centre line), and the one standard deviation of the estimates of the mean. The mean stabilizes after about 400 scenarios.

a deamplification of site response relative to the other sites. PSAR, ZOFR and COUR showed amplifications up to a factor of 6 at some frequencies. NEOK and SPLA were reference sites in the Ioannidou *et al.* study and, therefore, were considered natural in amplification. Station PEFK was not studied by Ioannidou *et al.*

These sites in the damage area are located in the up-dip direction of the presumed fault (Fig. 9). The sites where strong motion was recorded were more off-angle from the fault (except SPLA). Model 204 had a nearly unilateral rupture in the up-dip direction of the fault rupture. We concluded that the observed high intensities are caused by the combined site response and directivity effect of the fault rupture. Without site response, accelerations would have been in the 0.3-g range, as observed for NEOK and SPLA; however, this range is still greater in general than that obtained at the sites where motion was recorded. Without deamplification, MAGO would also have had accelerations in the 0.3-g range. These calculations automatically include the site effects identified by Assimaki *et al.* (2003).

Demonstration of a probabilistic seismic hazard study for Athens

We synthesized 500 earthquakes distributed throughout a source volume that is likely to have $M_w = 6.0$ earthquakes near Athens (discussed above, Fig. 2) so we could perform a limited probabilistic hazard study. Using HazStats, we generated 500 scenario earthquakes and used EMPSYN to synthesize three-component accelerograms for frequencies of 1.0 to 20.0 Hz at stations ATHA, DMKA, FIXA, THVC, SPLA and SGMA. We assumed an average return period of 1000 yr for an earthquake of this magnitude in the particular source zone and, thus, simulated a catalogue of ground motion for a period of 500 000 yr. In this demonstration, we did not include changes to the tectonic conditions for the time period. However, we assumed that every possible type of $M_w = 6.0$ earthquake that would occur had been modelled. This assumption requires a long enough time period for several earthquake cycles to occur at any particular location within the volume. We obtained a distribution of traditional ground-motion parameters such as peak acceleration or spectral ordinates from the synthesized ground motions and developed hazard curves in the form of the annual probability of exceedance. In future hazard studies, these types of ground motions might be used directly to build response models that calculate risk.

Fig. 12 shows the mean of the absolute acceleration response at a 0.5-s period as a function of the number of scenarios run. After about 400 scenarios, the mean stabilizes, indicating that our approach has captured the full variability for this region. Fig. 13 shows the plus-and-minus standard deviation of the distribution of Fourier amplitude spectra for the 500 models. Individual spectra are shown for only 100 models. The standard deviation represents the distribution of ground motion that could possibly affect the site.

Comparing Fig. 7 with Fig. 13 is instructive. Fig. 13 shows a broader distribution and generally lower values than Fig. 7, except at station THVC, where overall values increased. These effects are due to a greater distribution of distances, more sources farther away (or closer for THVC), and combinations of rupture that caused extreme ground motions. The effect of extreme ground motions is evident in spectra for stations SGMA, SPLA, ATHA, DMKA and FIXA. None of the stations used to acquire the Fig. 13 spectra is closer to the source than those used for Fig. 7; however, several (of only 100) have significantly higher amplitude ground motions.

Fig. 14 shows bar graphs of AAR at 0.5 s at the six sites. This figure represents the complete history of the ordinate values for 500 000 yr from magnitude 6.0 earthquakes (based on our assumptions). These values represent all factors that could affect the site and, thus, define the complete hazard. In Fig. 14, exaggerated vertical bars along the abscissa axes represent values where only one event contributed to the bar graph. These events tend to be outliers from the main distribution and represent 'extreme' events. Their values range from two to five times the standard deviation. Interestingly, a scenario that produces an extreme event at one station may not do so at other stations. Fig. 14 also shows the annual probability of exceedance from the 0.5-s AAR at the six sites, which is the PSHA at a specific ordinate from magnitude 6.0 earthquakes.

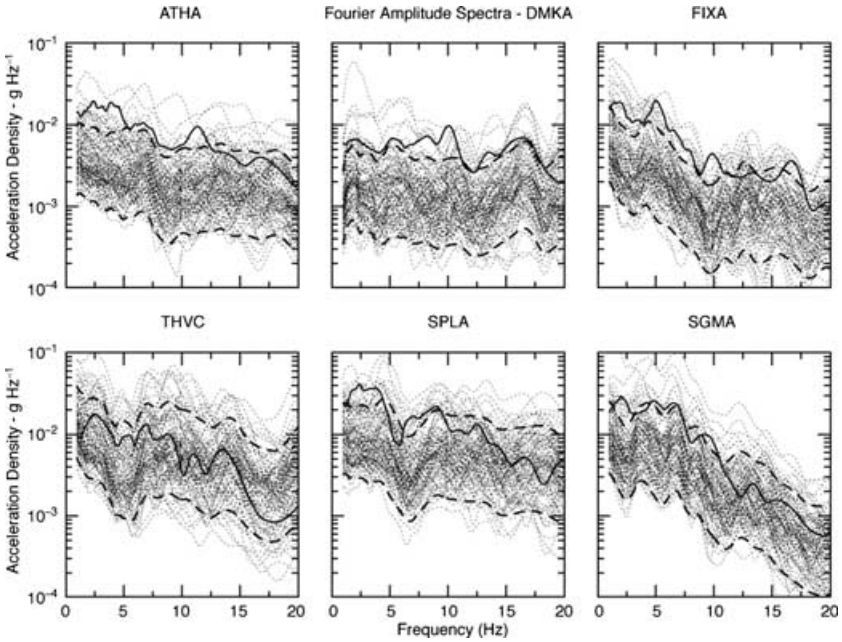

Figure 13. Fourier amplitude spectra for 100 of the 500 scenarios calculated (dotted line) in the larger source volume where the demonstration PSHA is performed; the plus-and-minus standard deviation values of the prediction (thick dashed lines); and the AAR recorded (thick solid line).

DISCUSSION AND CONCLUSIONS

In this paper, we presented a methodology to predict the range of ground-motion hazard for a fixed-magnitude earthquake along a specific fault or within a specific source volume. Our methodology is based on physical parameters that can be bounded by research, and thus, the uncertainty of the calculated hazard will be narrowed with more knowledge. We demonstrated how to apply this methodology to PSHA. Current approaches to hazard calculations use empirically derived parameters that are characterized by probability distributions. This results in parameters without boundaries, and no method is currently available to reduce the uncertainty.

We demonstrated our methodology with the 1999 Athens earthquake. We fixed the moment to that of the 1999 Athens earthquake and synthesized 57 rupture scenarios in a source volume estimated to be the likely location for an earthquake of this size near Athens. We developed constraints on rupture parameters based on prior knowledge of earthquake rupture processes and sources in the region and ran a sufficient number of scenario earthquakes to span the full variability of ground motion possible from our method. To provide EGFs, we used aftershocks ($M_w < 4.0$) that were larger than the criteria for having impulsive point sources and were distributed throughout the area. Using events that are not necessarily along the fault to be modelled is assumed to result in an average propagation path effect along with site-specific site response. This assumption appears to be validated because our results show that shapes of spectra match those observed. We also generated impulsive point source EGFs by deconvolution with a Brune source. Although this approach provides a wider range of events that can be used as EGFs, it needs further validation to be widely used.

The plus-one standard deviation of engineering parameters predicted by our model spans the actual event. The likelihood of an earthquake falling outside the plus-and-minus standard deviation values is thus 32 per cent, and the likelihood of having an Athens-type earthquake above the one-standard-deviation value is 16 per cent. However, the recorded events are approximately equal to the one-standard-deviation value, and only the high end of our synthesized seismograms match observed data. One of several hypotheses may explain why the fit is near the one-standard-deviation values for most stations. For example, the actual earthquake may have been an unusual event, or the event modelled may have actually been larger than the $M_w = 6.0$ assumed. The syntheses methodology may be systematically biased to low values, although a systematic bias has not been observed in previous validations for this methodology. Another possibility is that the location of stations has introduced a systematic bias. Five of the six stations are in a limited azimuth range and, thus, may reflect similar directional effects. A different configuration might change the results. The deconvolution with a Brune source to create EGFs is not considered a potential cause because we match shapes of spectra well and errors in deonvolution would only contribute to errors at high frequencies.

The range of the distributions in both the Fourier amplitude and acceleration response spectra is a factor of about plus-or-minus 4 (Figs 7 and 8). This is consistent with the worldwide database for earthquakes at a particular distance. However, we could narrow the range with more knowledge. Similarly, the worldwide database might show a smaller distribution if only specific faults were considered. Nonetheless, we feel that our distribution is narrow enough to be functionally useful for hazard analysis, and we provide a logical means to reduce the uncertainty by adding more knowledge.

The records generated by one of our source models matched the observed time histories well. Most of the rupture models that gave good fits to actual seismograms occurred in the vicinity of 38.05°N, 23.60°W, with the centre of rupture near a 12-km depth and showing nearly unilateral rupture toward the northeast of Athens. Strikes ranged from N107°E to N115°E, dips ranged from 39° to 48°, rupture velocity ranged from 0.92 to 0.99 times V_s. Rupture directivity, although partially toward Athens, was primarily in the direction of the highest damage areas. The slip distribution of our best models agreed well with those of previous studies. The fit to seismograms

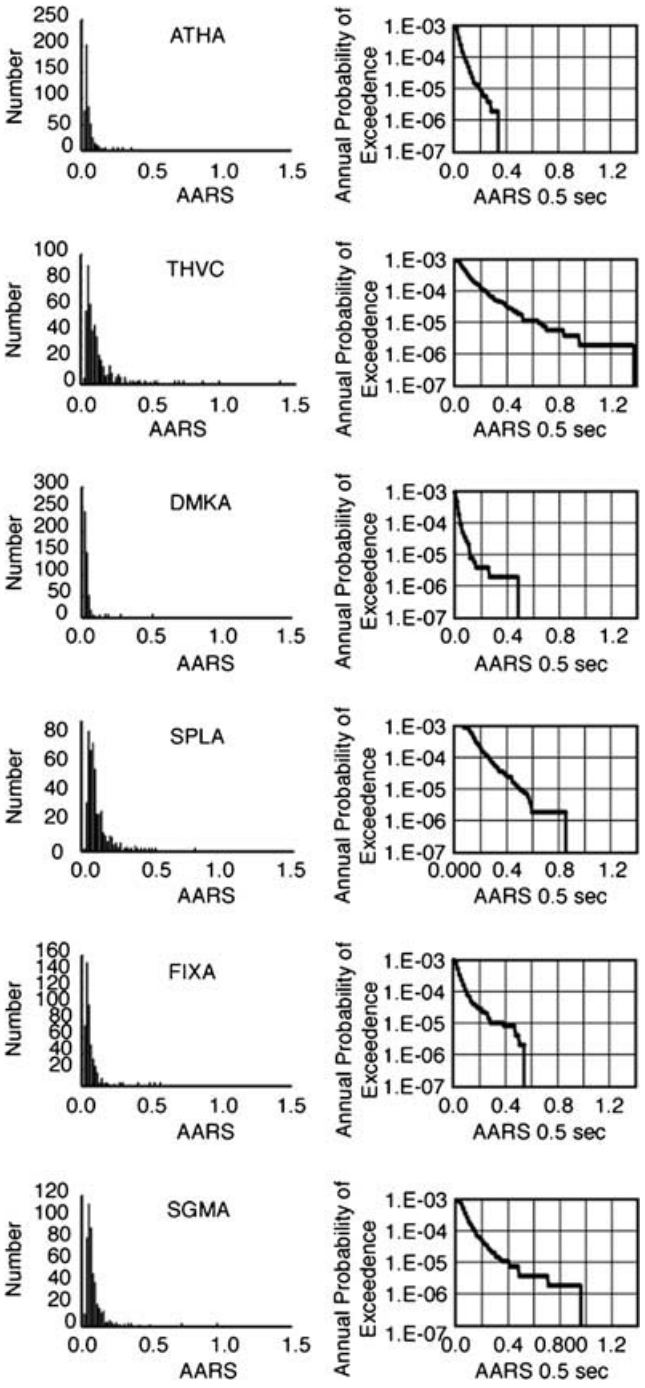

Figure 14. The histogram (left) of AAR values at 0.5 s and the resulting hazard curve (right). The axes for the histogram extend to 'extreme' values because certain combinations of rupture parameters result in high ground motions at some stations. These 'extremes' are indicated by exaggerated vertical bars on the abscissa because the scale is too large to show their contribution to the histogram.

indicates that, for engineering purposes, this methodology can provide realistic ground-motion information in advance of an earthquake, including a model of what will actually happen. In addition, the computer programs COMPARE, HAZARD and EMPSYN might be used in an inversion scheme to determine the rupture scenario of a previous earthquake based upon recordings of aftershocks.

We also synthesized strong-motion records in high-damage areas for which records do not exist. Peak accelerations ranged from about 0.2 g at station MAGO to 0.4 g at stations COUR, STEF and ZOFR to 0.7 g at PEFK and PSAR. Stations COUR, ZOFR and PEFK are near the highest intensity values from this earthquake (Fig. 2) and have relatively high peak accelerations. Our best-fitting rupture models showed a strong unilateral rupture up dip toward these sites. This rupture, along with higher site response, may have caused the high damage in this area.

We developed the demonstration PSHA for a magnitude 6.0 earthquake using synthesized records to represent a long enough period of history so that all possible earthquakes have occurred. The program HazStats compiles the distribution of traditional ground-motion parameters such as peak acceleration or spectral ordinates that simulate the actual record of ground motion for this time period, and uses this distribution to develop hazard curves in the form of the annual probability of exceedance. All of the necessary elements to conduct PSHA studies with synthesized ground motion are in place and need only to be implemented in a systematic way to capture the epistemic and aleatory uncertainty. The true application of the methodology demonstrated here is to extend the work to a full range of moments and all possible sources and use the results to conduct a full synthetic probabilistic hazard study.

We observed outliers from the main distribution, which represent 'extreme' events. Their values range from two to five times the standard deviation. However, rather than increasing with long time periods, they get replicated, so that, in effect, the distributions of ground motion are naturally truncated by the physics of the earthquake cycle.

ACKNOWLEDGMENTS

George Stavrakakis provided leadership in bringing these collaborators together. Jean Savy provided detailed expertise on probabilistic hazard assessment. We benefited from discussions with Paul Kasameyer. We benefited greatly by thorough reviews by two anonymous reviewers. This project was partially funded by the National Observatory of Athens, Greece, which also contributed significant data and data processing. The University of Athens, Greece contributed significant computational facilities and data. This project was partially supported by the University of California, Lawrence Livermore National Laboratory under the auspices of the U.S. Department of Energy under contract W-7405-Eng-48.

REFERENCES

Abrahamson, N.A. & Shedlock, K.M., 1997. Overview, *Seismol. Res. Lett.,* **68**(1).

Abrahamson, N.A., Somerville, P.G. & Cornell, C.A., 1990. Uncertainty in numerical strong motion predictions, in *Proc. Fourth U.S. National Conf. Earthquake Engineering,* Vol. 1, Earthquake Engineering Research Institute, 20–24 May, Palmsprings, California.

Aki, K. & Richards, P.G., 1980. *Quantitative Seismology, Theory and Methods*,Vol. I–II, W.H. Freeman and Company, San Francisco, CA.

Anderson, J.G., 2003. Quantitative measure of the goodness of fit of synthetic accelerograms, *presented at 13th World Conference on Earthquake Engineering*, Vancouver, B.C., Canada, August 1–6, 2004, paper No. 243.

Anderson, J.G. & Brune, J., 1999. Probabilistic seismic hazard analysis without the ergodic assumption, *Seismol. Res. Lett.,* **71**(1), 19–28.

Assimaki, D., Gazetas, G. & Kausel, E., 2003. Effects of local soil conditions on the topographic aggravation of seismic motion: parametric

investigation and recorded field evidence from the 1999 Athens earthquake, *Bull. seism. Soc. Am.,* **95**, 1059–1089.

Basili, M. & Brady, G., 1978. Low frequency filtering and the selection of limits for accelerogram corrections, *Proc. VI European Conf. Earthquake Engineering*, September 18–22, Dubrovnik, Yugoslavia, pp. 251–258.

Boatwright, J.L., 1981. Quasi-dynamic models of simple earthquake: an application to an aftershock of the 1975 Oroville, California earthquake. *Bull. seism. Soc. Am.,* **71**, 69–94.

Bommer, J.J. *et al.,* 2004. The challenge of defining upper bounds on earthquake ground motion, *Seismol. Res. Lett.,* **75**(1), 82–95.

Boore, D., 1983. Stochastic simulation of high-frequency ground motions based on seismological models of the radiated spectra, *Bull. seism. Soc. Am.,* **73**(6), 1865–1894.

Burridge, R. & Willis, J.R., 1969. The self-similar problem of the expanding crack in an anisotropic solid, *Proc. Cambridge Phil. Soc.,* **66,** 443–468.

Campbell, K.W. & Bozorgnia, Y., 2003. Updated near-source ground-motion (attenuation) relations for the horizontal and vertical components of peak ground acceleration and acceleration response spectra, *Bull. seism. Soc. Am.,* **93,** 314–331.

Cohee, B.P., Somerville, P.G. & Abrahamson, N.A., 1991. Simulated ground motions for hypothesized $M_w = 8.0$ subduction earthquakes in Washington and Oregon, *Bull. seism. Soc. Am.,* **81,** 28–56.

Convertito, V., Emolo, A. & Zollo, A., 2006. Seismic-hazard assessment for a characteristic earthquake scenario: an integrated probabilistic-deterministic method, *Bull. seism. Soc. Am.,* **96,** 377–391.

Cornell, C.A., 1968. Engineering seismic risk analysis, *Bull. seism. Soc. Am.,* **58,** 1583–1606.

Dan, K., Watanabe, T., Tanaka, T. & Sato, R., 1990. Stability of earthquake ground motion synthesized by using different small-event records as empirical Green's functions, *Bull. seism. Soc. Am.,* **80,** 1433–1455.

Douglas, J., 2003. Earthquake ground motion estimation using strong-motion records: a review of equations for the estimation of peak ground acceleration and response spectral ordinates, *Earth-science Reviews,* **61,** 43–104.

EERI, 1999. The Athens, Greece earthquake of September 7, 1999, *Special Earthquake Report—Learning from Earthquakes*, EERI, November 1999.

Fenves, G.L. & Ellery, M., 1998. *Behavior and Failure Analysis of a Multiple-Frame Highway Bridge in the 1994 Northridge Earthquake*, Pacific Earthquake Engineering Research Center, Report No. PEER 98/08.

Field, E.H. & the Phase II Working Group, 2000. Accounting for site effects in probabilistic seismic hazard analyses of southern California: overview of the SCEC Phase II Report, *Bull. seism. Soc. Am.,* **90,** S1–S31.

Field, E.H., Jordan, T.H. & Cornell, C.A., 2003. OpenSHA: a developing community-modeling environment for seismic hazard analysis, *Seism. Res. Lett.,* **74**(4), 406–419.

Foxall, W., Hutchings, L. & Kasameyer, P., 1994. Lithological and rheological constraints on fault rupture scenarios for ground motion hazard prediction, *IUTM Symp. Mechanics Problems in Geodynamics*, September 5–9, 1994, Beijing, China; also published by Lawrence Livermore National Laboratory, Livermore, CA, UCRL-JC-116437.

Gok, R. & Hutchings, L., 2006. Source parameters and Scaling Relations for the North Anatolian fault zone, Turkey Earthquake, submitted, *Bull. seism. Soc. Am.,* LLNL, UCRL-JC-206080.

Guatteri, M.P., Mai, M., Beroza, G.C. & Boatwright, J., 2003. Strong ground-motion prediction from stochastic-dynamic source models, *Bull. seism. Soc. Am.,* **93,** 301–313.

Hald, A., 1952. *Statistical theory and engineering applications*, John Wiley and Sons, New York.

Hanks, T.C. & Kanamori, H., 1979. A moment magnitude scale, *J. geophys. Res.,* **84,** 2348–2350.

Hartzell, S.H., 1982. Simulation of ground accelerations for May 1980 Mammoth Lakes, California, earthquakes, *Bull. seism. Soc. Am.,* **72,** 2381–2387.

Hartzell, S., Harmsen, S., Frankel, A. & Larsen, S., 1999. Calculation of broadband time histories of ground motion: comparison of methods and validation using strong-ground motion from the 1994 Northridge earthquake. *Bull. seism. Soc. Am.,* **89,** 1484–1504.

Heaton, T.H., 1982. The 1971 San Fernando earthquake: a double event? *Bull. seism. Soc. Am.,* **72,** part A, 2037–2063.

Heuze, F.E., Ueng, T.S., Hutchings, L.J., Jarpe, S.P. & Kasameyer, P.W., 1994. A coupled seismic-geotechnical approach to site-specific strong motion, *Soil Dyn. Earthq. Eng.,* **16**(4), 259–272.

Hutchings, L., 1991. 'Prediction' of strong ground motion for the 1989 Loma Prieta earthquake using empirical Green's functions, *Bull. seism. Soc. Am.,* **81,** 88–121.

Hutchings, L., 1994. Kinematic earthquake models and synthesized ground motion using empirical Green's functions, *Bull. seism. Soc. Am.,* **84,** 1028–1050.

Hutchings, L., 2004. *Program NetMoment, a Simultaneous Inversion for Moment, Source Corner Frequency, and Site Specific t**, Lawrence Livermore National Laboratory, Livermore, CA, UCRL-ID-135693.

Hutchings, L. & Jarpe, S., 1996. Ground-motion variability at the Highway 14 and I-5 interchange in the northern San Fernando Valley, *Bull. seism. Soc. Am.,* **86,** S289–S299.

Hutchings, L. & Wu, F., 1990. Empirical Green's functions from small earthquakes: a waveform study of locally recorded aftershocks of the San Fernando earthquake, *J. geophys. Res.,* **95,** 1187–1214.

Hutchings, L., Ioannidou, E., Jarpe, S. & Stavrakakis, G.N., 1997. *Strong Ground Motion Synthesis for a* M = 7.2 *Earthquake in the Gulf of Corinth, Greece Using Empirical Green's Functions*, Lawrence Livermore National Laboratory, Livermore, CA, UCRL-JC-129394.

Hutchings, L.J., Jarpe, S.P., Kasameyer, P.W. & Foxall, W., 1996. Synthetic strong ground motions for engineering design utilizing empirical Green's functions, *Proc. Fourth Caltrans Seismic Research Workshop*, p. 24; also presented at Eleventh World Conference of Earthquake Engineering, Acapulco, June 23–28, 1996 (CDROM Elsevier); available from Lawrence Livermore National Laboratory, Livermore, CA, UCRL-JC-123762.

Hutchings, L., Jarpe, S. & Kasameyer, P., 1998. *Validation of a Ground Motion Synthesis and Prediction Methodology for the 1988,* M = 6.0, *Saguenay Earthquake*, Lawrence Livermore National Laboratory, Livermore, CA, UCRL-JC-129395.

Hutchings, L., Kasameyer, P.W. & Foxall, W., 2003. *LLNL Hazard Mitigation Center Ground Motion Prediction Methodology*, Lawrence Livermore National Laboratory, Livermore, CA, UCRL-ID-135697.

Hutchings, L., Foxall, B., Kasameyer, P., Larsen, S., Hayek, C., Tyler-Turpin, C., Aquilino, J. & Long, L., 2005. *Deep Borehole Instrumentation along San Francisco Bay Bridges: 1996–2003 and Strong Ground Motion Synthesis along the San Francisco/Oakland Bay Bridge, Final Report*, Lawrence Livermore National Laboratory, Livermore, CA, UCRL-TR-217303.

Ioannidou, E., Voulgaris, N., Kalogeras, I., Hutchings, L. & Stavrakakis, G., 2001. Analysis of site response in the Athens area from the 7 September 1999, $M_w = 5.9$ Athens earthquake and aftershock recordings, and intensity observations, *Bollettino di Geofisica Teorica ed Applicata*, Special Issue on Site Response, December 2001.

Jarpe, S.J. & Kasameyer, P.K., 1996. Validation of a methodology for predicting broadband strong motion time histories using kinematic rupture models and empirical Green's functions, *Bull. seism. Soc. Am.,* **86,** 1116–1129.

Katsikatsos, G., Migiros, G., Triandaphyllis, M. & Mettos, A., 1986. Geological structure of internal Hellenides, *Geolog. Geophys. Res. Special Issue,* pp. 191–212, IGME, Athens.

Kontoes, C., Elias, P., Sykioti, O., Briole, P., Remy, D., Sachpazi, M., Veis, G. & Kotsis, I., 2000. Displacement field and fault model for the September 7, 1999, Athens earthquake inferred from ERS2 Satellite radar interferometry, *Geophys. Res. Lett.,* **27,** 3989–3992.

Kostrov, B.V. & Das, S., 1988. Principles of earthquake source mechanics, in *Cambridge Monographs on Mechanics and Applied Mathematics,* Cambridge University Press, Cambridge, UK.

Lee, W.H.K., Shin, T.C., Kuo, K.W., Chen, K.C. & Wu, C.F., 2001. CWB free-field strong-motion data from the 21 September Chi-Chi, Taiwan, earthquake, *Bull. seism. Soc. Am.,* **91,** 1370–1376.

Louvari, E. & Kiratzi, A., 2001. Source Parameters of the September 7, 1999, Athens earthquake based on teleseismic data, J. Balkan, *Geophys. Soc.,* **4,** 51–56.

Makropoulos, K., Drakopoulos, J. & Kouskoun, V., 1989. The earthquake sequence in Volos, central Greece, April 30, 1985. Analysis of strong motion, *IASPEI* (Abstracts), Istanbul.

Mariolakos, I. & Foundoulis, I., 2000. The Athens earthquake September 7, 1999, the neotectonic regime of the affected area, *Ann. Geol. Pay Helleniques,* Tom. XXXVIII, Fasc. B.

Mayeda, K., Hofstetter, A., O'Boyle, J.L. & Walter, W.R., 2003. Stable and transportable regional magnitudes based on coda-derived moment-rate spectra, *Bull. seism. Soc. Am.,* **93**(1), 224–239.

McCallen, D., Astaneh-Asl, A., Larsen, S. & Hutchings, L., 2006. Dynamic response of the suspension spans of the San Francisco–Oakland Bay Bridge, p. 19, *Proc. EERI Conf.*, San Francisco, CA, April 2006.

National Research Council, 2003. *Living on an Active Earth: Perspectives on Earthquake Science*, National Academic Press, Washington, D.C.

Orowan, E., 1960. Mechanism of seismic faulting, *Geol. Soc. Am. Bull.,* **79,** 323–345.

Papadimitriou, P., Kassaras, G., Voulgaris, N., Kassaras, I., Delibasis, N. & Makropoulos, K., 2000. The September 7, 1999 Athens earthquake sequence recorded by the Cornet network: preliminary results of source parameters determination of the mainshock, *Ann. Geol. des Pay Helleniques,* Tom. XXXVIII, Fasc. B.

Papadopoulos, G.A., Drakatos, G., Papanastassiou, D., Kalogeras, I. & Stavrakakis G., 2000. Preliminary results about the catastrophic earthquake of 7 September 1999 in Athens, Greece, *Seismol. Res. Lett.,* **71**(3), 318–329.

Papageorgiou, A.S. & Aki, K., 1983. A specific barrier model for the quantitative description of inhomogeneous faulting and the prediction of strong ground motion, I, description of the model, *Bull. Seism. Soc. Am.,* **73,** 693–722.

Papazachos, C., 1992. Anisotropic radiation modeling of macroseismic intensities for estimation of the attenuation structure of the upper crust in Greece, *Pageoph,* **138,** 445–469.

Papazachos, V. & Papazachov, K., 1997. The Earthquakes of Greece: Thessaloniki: Editions. Ziti.

Pavic, R., Koller, M.G., Bard, P.-Y. & Lacave-Lachet, C., 2000. Ground motion prediction with the empirical Green's function technique: an assessment of uncertainties and confidence level, *J. Seismol.,* **4,** 59–77.

Pavlides, S.B., Papadopoulos, G. & Ganas, A., 2002. The fault that caused the Athens September 1999, $M_s = 5.9$ earthquake: field observations, *Natural Hazards.,* **27,** 61–84.

Protonotarios, I., 1999. Preliminary conclusions from the September 7, 1999 earthquake, *Workshop on the September 7, 1999, Athens Earthquake,* November 2, 1999, Athens, Greece.

Rosset, Ph., Wagner, J.-J., Garcia-Fernandez, M. & Jimenez, M.J., 1998. *Strong Ground Motion Simulation with Empirical Green's Functions; First Attempts in the Framework of the European Project SERGISAI*. EC Environment Research Programme, Climatology and Natural Hazards (1994–1998).

Roumelioti, Z., Dreger, D., Kiratzi, A. & Theodoulidis, N., 2003. Slip distribution of the 7 September 1999 Athens earthquake inferred from empirical Green's function study, *Bull. seism. Soc. Am.,* **93,** 775–782.

Roumelioti, Z., Kiratzi, A. & Theodoulidis, N., 2004. Stochastic strong ground motion simulation of the 7 September 1999 Athens (Greece) earthquake, *Bull. seism. Soc. Am.,* **94,** 1036–1052.

Schulz, C.H., 2002. *The Mechanics of Earthquakes and Faulting*, Cambridge University Press, New York, NY, p. 471.

Scognamiglio, L., 2004. A test of ground motion prediction methods that utilize small earthquakes, *PhD dissertation*, Institute of Volcanology and Geophysics, Rome, Italy.

Scognamiglio, L., Hutchings, L., Akinci, A. & Foxall, W., 2005. Finite source strong ground motion synthesis with pseudo Green's functions, *Abs. Am. Geophys. Union*, San Francisco.

Sibson, R.H., 1982. Fault Zone Models, Heat Flow and the Depth Distribution of Earthquakes in the Continental Crust of the United States, *Bull. seism. Soc. Am.,* **72,** 151–16.

Somerville, P. *et al.,* 1999. Characterizing crustal earthquake slip models for the prediction of strong ground motion, *Seism. Res. Lett.,* **70**(1), 59–80.

Spudich, P. & Frazier, L.N., 1984. Use of ray theory to calculate high-frequency radiation from earthquake sources having spatially variable rupture velocity and stress drop, *Bull. seism. Soc. Am.,* **74,** 2061–2082.

Stavrakakis, G., 1999. The Athens earthquake of September 7, 1999, *Newsletter of the European Centre on Prevention and Forecasting of Earthquakes,* **3,** 26–29.

Stavrakakis, G.N., Kalogeras, I.S. & Drakopoulos, J.C., 1993. Preliminary analysis of Greek accelerograms recorded at stations of NOA's network: time period 1973–1990, *Proc. 2nd Congress Hellenic Geophys. Union*, Florina, Greece, 5–7 May, pp. 175–191.

Steidl, J.H., Tumarkin, A.G. & Archuleta, R.J., 1996. What is a reference site? *Bull. seism. Soc. Am.,* **86,** 1733–1748.

Trifunac, M.D. & Lee, V.W., 1973. Routine computer processing of strong-motion accelerograms, *EERI,* **73**(03).

Tse, S.T. & Rice, J.R., 1986. Crustal earthquake instability in relation to the depth variation of frictional slip properties, *J. geophys. Res.,* **91,** 9452–9472.

Tselentis, G-A. & Zahradnik, J., 1999. Aftershock monitoring of the Athens earthquake of 7 September 1999, *Seism. Res. Lett.,* **71**(3), 330–337.

Tumarkin, A., 1997. Energy constraints on synthesis of strong ground motion, *Abs. Am. Geophys. Union*, San Francisco.

Voulgaris, N., Kassaras, I., Papadimitriou, P. & Delibasis, N., 2000. Preliminary results of the Athens September 7, 1999 aftershock sequence, *Ann. Geol. des Pay Helleniques,* Tom. XXXVIII, Fasc. B.

Wells, D.L. & Coppersmith, K.J., 1994. New empirical relationships among magnitude, rupture length, rupture width, rupture area, and surface displacement, *Bull. seism. Soc. Am.,* **84,** 974–1002.

Wossner, J., Treml, M. & Wenzel, F., 2002. Simulation of $M_w = 6.0$ earthquakes in the Upper Rhinegraben using empirical Green functions, *Geophys. J. Int.,* **151,** 487–500.

Zollo, A., Bobbio, A., Emolo, A., Herreo, A. & De Natale, G., 1997. Modeling of ground acceleration in the near source range: the case of the 1976, Friuli earthquake ($M = 6.5$), northern Italy, *J. Seismol.,* **1,** 305–319.